Structure

Article

Design of multi-target peptide modulators for protein chaperone networks

Graphical abstract

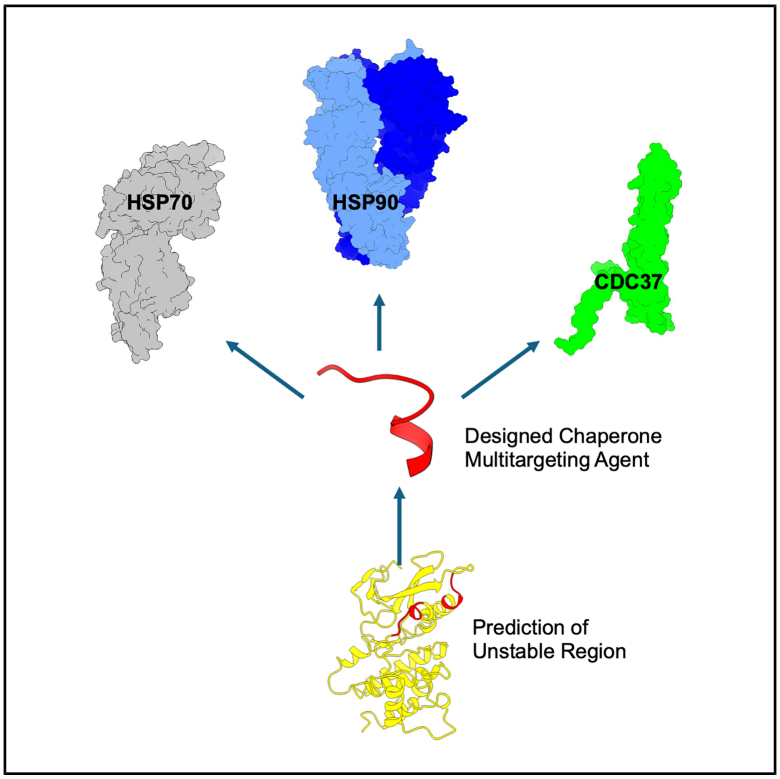

Authors

Luca Torielli, Matteo Castelli, Francesca Milani, ..., Jason E. Gestwicki, Mehdi Mollapour, Giorgio Colombo

Correspondence

jason.gestwicki@ucsf.edu (J.E.G.), mollapom@upstate.edu (M.M.), g.colombo@unipv.it (G.C.)

In brief

Torielli et al. describe a computational approach that allows the identification of peptide Cdk4-2 to dually inhibit the molecular chaperones Hsp70 and Hsp90. This multi-target inhibitor binds the targets, prevents oncoprotein activation, and induces cell death in renal cancer cells, presenting a promising new strategy for developing drugs against complex protein networks.

Highlights

- Integrated design approach to peptides that simultaneously inhibit Hsp70 and Hsp90
- Designed peptide binds Hsp70, Hsp90, and co-chaperone Cdc37 as multi-target inhibitor
- The design shows promising anti-cancer effects
- Rational, broadly applicable strategy to disrupt or modulate protein networks

Torielli et al., 2025, Structure *33*, 1944–1957
November 6, 2025
https://doi.org/10.1016/j.str.2025.07.021

CellPress

CellPress
OPEN ACCESS

Structure

Article

Design of multi-target peptide modulators for protein chaperone networks

Luca Torielli,[1,12] Matteo Castelli,[1,12] Francesca Milani,[1,12] Jennifer A. Heritz,[2,3,4] Sara J. Cayaban,[2,3,4] Jason Hernandez,[9] Stefano A. Serapian,[1] Andrea Magni,[1] Elena Frasnetti,[1] Filippo Doria,[1] Valentina Pirota,[1] Laura A. Wengert,[2,3] Mark R. Woodford,[2,3,4] Giulia Lodigiani,[5] Greta Bergamaschi,[5] Marina Veronesi,[6] Tiziano Bandiera,[7] Stefania Girotto,[6] Antonella Paladino,[8] Chrisostomos Prodromou,[10] Sarah J. Backe,[2,3] Dimitra Bourboulia,[2,3,4] Anselmo Canciani,[11] Cristina Arrigoni,[11] Marco Lolicato,[11] Jason E. Gestwicki,[9,*] Mehdi Mollapour,[2,3,4,*] and Giorgio Colombo[1,13,*]

[1]Department of Chemistry, University of Pavia, Via Taramelli 12, 27100 Pavia, Italy
[2]Department of Urology, SUNY Upstate Medical University, Syracuse, NY 13210, USA
[3]Upstate Cancer Center, SUNY Upstate Medical University, Syracuse, NY 13210, USA
[4]Department of Biochemistry and Molecular Biology, SUNY Upstate Medical University, Syracuse, NY 13210, USA
[5]National Research Council of Italy, Istituto di Scienze e Tecnologie Chimiche "Giulio Natta" (SCITEC-CNR), Via Mario Bianco 9, 20131 Milano, Italy
[6]Structural Biophysics Facility, Istituto Italiano di Tecnologia, Via Morego 30, 16163 Genova, Italy
[7]D3 PharmaChemistry, Istituto Italiano di Tecnologia, Via Morego 30, 16163 Genoa, Italy
[8]Institute of Biostructures and Bioimaging, CNR, Via Pietro Castellino 111, 80131 Naples, Italy
[9]Department of Pharmaceutical Chemistry and the Institute for Neurodegenerative Diseases, University of California, San Francisco, San Francisco, CA 94158, USA
[10]Biochemistry and Biomedicine, School of Life Sciences, University of Sussex, Falmer, BN1 9QG Brighton, UK
[11]Department of Molecular Medicine, University of Pavia, Via Ferrata 2, 27100 Pavia, Italy
[12]These authors contributed equally
[13]Lead contact
*Correspondence: jason.gestwicki@ucsf.edu (J.E.G.), mollapom@upstate.edu (M.M.), g.colombo@unipv.it (G.C.)
https://doi.org/10.1016/j.str.2025.07.021

SUMMARY

Essential chaperones heat shock protein 70 (Hsp70) and heat shock protein 90 (Hsp90) collaborate in oncoprotein folding. Dual inhibition of these chaperones has shown synergy in preclinical studies but remains challenging to achieve. Using a computational approach, we designed peptides mimicking the predicted unfolding regions of Kinase CDK4, a client protein of both Hsp70 and Hsp90. Peptide Cdk4-2 is shown to simultaneously bind Hsp70, Hsp90, and co-chaperone Cdc37. Cdk4-2 is membrane permeable, inhibits CDK4-mediated retinoblastoma phosphorylation, and induces apoptosis in renal carcinoma cells. Structure-function studies identified a minimal pharmacophore for Hsp70 binding and critical interactions for peptide affinity. These findings demonstrate the feasibility of rationally designing multi-target modulators of chaperone networks. Cdk4-2 is a promising lead for therapeutic development, expanding the molecular space of modulators of cancer-associated multiprotein machineries. While focused on chaperones, the idea behind our strategy is general and immediately transferable to other multiprotein targets and networks.

INTRODUCTION

Protein quality control is maintained through the function of molecular chaperones, including Hsp70 and Hsp90.[1] While Hsp70 and Hsp90 are important for cellular health under normal conditions, they become especially critical during tumorigenesis by playing roles in angiogenesis, metastasis, and cell survival.[2–7] To exploit this susceptibility, chemical inhibitors of Hsp70 and Hsp90 have been explored as potential anti-cancer agents. Recently, an Hsp90 inhibitor, pimitespib (Jeselhy, TAS-116), demonstrated positive outcomes in a randomized phase III clinical trial and gained approval for treating advanced gastrointestinal stromal tumor (GIST) in Japan.[8] However, it is known that many inhibitors of Hsp90 trigger an upregulation of Hsp70 expression, partially compensating for the loss of Hsp90 activity and sustaining prosurvival signaling pathways.[9,10] Indeed, despite the promising results with pimitespib, most Hsp90 inhibitors have failed in the clinic,[11] emphasizing the need for alternative therapeutic strategies.

One compelling idea is that targeting both Hsp70 and Hsp90 at the same time might enhance efficacy. In support of this idea, many studies have shown synergy between combinations of Hsp70 and Hsp90 inhibitors.[2–7,12] While these findings are motivational, clinical development of a cocktail of Hsp70 and Hsp90 inhibitors is expected to be challenging. Here, we investigate the alternative possibility of simultaneously targeting

both chaperones with a dual-targeting compound. Briefly, multi-targeting compounds use rationally designed promiscuity to bind and inhibit (at least) two targets, and select examples have been approved in oncology.[13] The challenge in the design of these compounds is to identify a core pharmacophore that is malleable enough to be adapted for both targets.

Hsp90 and Hsp70 directly bind to exposed sequences in the unfolded or partially folded states of their ''client'' proteins. The selection of these clients is often further supported by co-chaperones, such as Cdc37 and J-domain proteins.[14] For example, Cdc37 is required to recruit Hsp90 into complexes with kinases,[15] but not other clients. For a subset of clients, the Hsp90 and Hsp70 complexes are known to work sequentially on the same polypeptide. For example, pioneering work on steroid hormone receptors has revealed that Hsp70 and its co-chaperones generally bind the unfolded client first, followed by recruitment of Hsp90 and its associated factors.[16,17] These sequential protein-protein interactions between chaperones, co-chaperones and client proteins then prepare the client for final folding.[18,19] This process appears to be critical for folding and stability, as treatment with chemical inhibitors of Hsp70 or Hsp90 leads to destabilization and degradation of many clients.[20]

Guided by these observations, we envisioned that one way to simultaneously inhibit both Hsp90 and Hsp70 would be to identify shared binding sites on a client and then convert these sequences into peptide-based inhibitors. The challenge with this idea is that, to date, no peptides have been shown to bind both Hsp90 and Hsp70. Further, there are not tools for predicting these shared sites based solely on sequence information. Thus, we envisioned a different approach to this problem. Specifically, we previously demonstrated the capability of physics-based computation[21] to identify relatively unstable substructures in a client that are most likely to unfold. This *ab initio* prediction returned substructures that were shown to correspond to known, Hsp90-contacting regions of kinases and glucocorticoid receptor. Moreover, we were able to use structure-based approaches to design peptides that mimic these unfolding regions and found that they bound to Hsp90 and limited Hsp90-mediated client stabilization.[22] Because Hsp70 also binds to unstructured regions of proteins,[23] we hypothesize here that a similar approach might identify peptides that bind both Hsp70 and Hsp90, providing the starting point for dual-targeting molecules.

To test this idea, we selected the cyclin-dependent kinase, CDK4, as a model. CDK4 plays a pivotal role in oncogenesis by regulating the cell cycle and promoting cell proliferation through its involvement in G1 phase progression.[24,25] Aberrant activation or overexpression of CDK4 is commonly observed in various cancers, contributing to uncontrolled cell division and tumor development. Importantly, CDK4 is also a well characterized client of both Hsp70 and Hsp90 and substantial structural information for CDK4 in complex with Hsp90 is now available.[26,27] To identify shared binding sites for Hsp90 and Hsp70 on CDK4, we used our physics-based approach[21] to nominate four short peptides (termed **Cdk4-1** through **Cdk4-4**) that mimic the most unstable substructures in the kinase. Then, we synthesized the corresponding peptides and measured binding to Hsp90 and the co-chaperone Cdc37. We find that two of these sequences indeed bind both Hsp90 and Cdc37. Then, we show that one of these CDK4-derived peptides, **Cdk4-2**, also binds to Hsp70, with a tight affinity (K_i ~100 nM). Using a biotinylated version of **Cdk4-2**, we confirm that the peptide binds Hsp70 and Hsp90 in cell lysates. Finally, we find that **Cdk4-2** is partially membrane permeable, allowing us to show that treatment of renal cell carcinoma cells with **Cdk4-2**, but not a scrambled control, leads to suppression of CDK4 phosphorylation of its substrate Retinoblastoma (Rb) and activation of apoptosis. Thus, although further development is needed, **Cdk4-2** appears to be an exciting starting point for development of rationally designed, multitargeted molecules that inhibit interactions within the Hsp90 and Hsp70 chaperone complexes.

RESULTS

Design of peptides mimicking the unfolded regions of Cdk4

Hsp90 and Hsp70 share a number of client proteins; however, a peptide region that binds both chaperones has not yet been identified. To predict these peptides we envisioned a computational approach to identify unstable and unfolding-prone substructures in a client, with the hypothesis being that such regions might be likely targets for chaperone binding. We selected CDK4 as a target client as it is implied in a number of cancer processes.[25] Our protocol to identify potentially unfolding regions involves running a preliminary Molecular Dynamics (MD) simulation on the selected protein to allow the structure to relax strain and bad clashes that may be present in the initial crystal structure. In the present case, we used the trajectories of the simulations previously described by Paladino et al.[28] Next, on the representative structure of the most populated conformational cluster from such simulations, we computed pairwise interactions between residues via the Matrix of Low Energy Coupling, MLCE, approach,[21,29] which decomposes the nonbonded part of the potential (see STAR Methods): for a protein of N residues, an $N \times N$ interaction matrix M_{ij} is calculated. Eigenvalue decomposition of this matrix returns the regions of strongest and weakest couplings, such that the fragments that are on the surface, contiguous in sequence space and weakly coupled to the protein core, defining the potential chaperone-interacting regions. This approach identified four substructures, termed **Cdk4-1**, **Cdk4-2**, **Cdk4-3** and **Cdk4-4**, which are located on surface-exposed regions of CDK4 (Figure 1). These regions vary in sequence, except for **Cdk4-2** and **Cdk4-4**, where **Cdk4-4** is a subset of the longer **Cdk4-2** (Table 1). Table 1 presents the sequences of the identified peptides, their labels and the length of the simulations we ran for each of them, described in the next paragraph. These sequences were selected for successive experimental investigations.

The conformational landscape of designed peptides and their recognition of Hsp70 and Hsp90

As both Hsp90 and Hsp70 make contact with elongated, disordered sequences, we first explored whether any of the four sequences might adopt these conformations using molecular dynamics (MD) simulations. To this end, we performed all-atom molecular dynamics (MD) simulations for each sequence, running 40 independent replicas of 600 nanoseconds each.

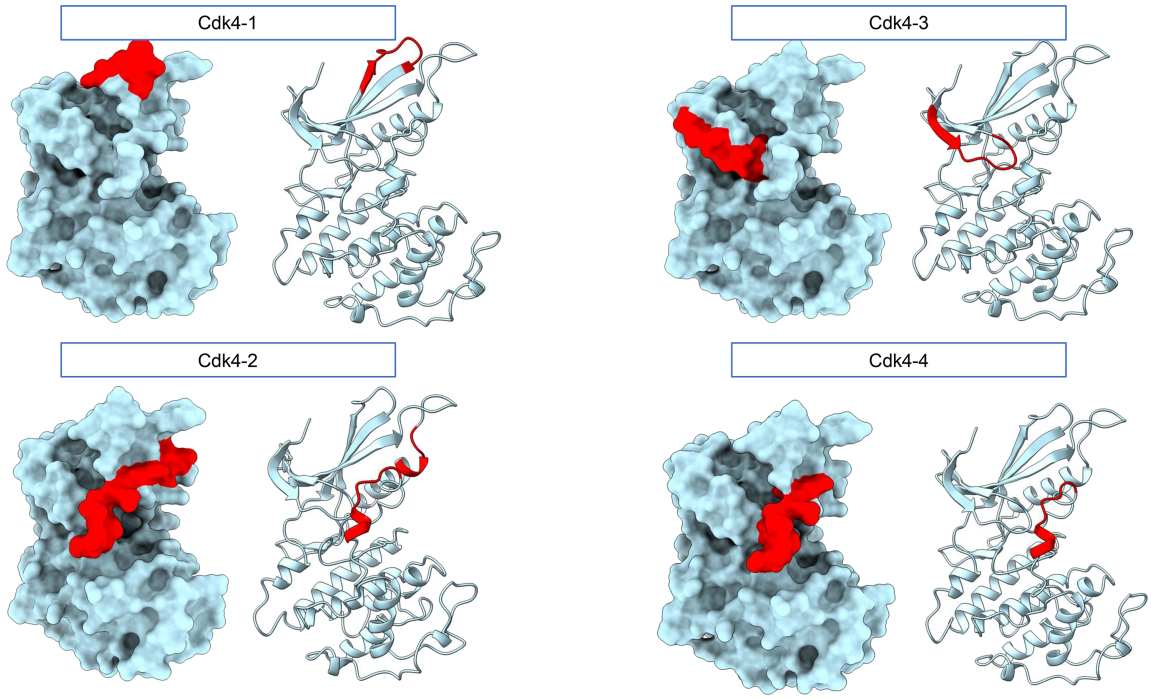

Figure 1. Predicting minimal mimics of unfolding regions on CDK4

The folded 3D structure of CDK4 (PDB: 3G33) is shown both with a surface (left) and secondary structure (right) representation. The four subpanels indicate the location and the structure of the regions predicted to be the minimal regions that are most prone to unfolding (red).

This resulted in 24 microseconds of sampling per peptide, and a combined total of 96 microseconds of simulation data. The distinct trajectories were separately analyzed by comparing the conformations populated by the peptides in solution to those observed in the native protein or in the cryo-EM structure of the Hsp90/CDK4/Cdc37 complex.[26] However, given the intrinsic flexibility of short peptides in solution, these simulations produced a large ensemble of structurally diverse conformations. Traditional clustering methods are often insufficient to resolve the complexity of such systems or to quantify the energetics and relevance of individual conformations. Therefore, to obtain a more energetically informed description of the peptide behavior, we employed Markov State Models (MSMs) analysis (details of MSMs construction and validation are provided in the STAR Methods section and supplemental information). MSMs resolved the thermodynamic and kinetic properties of distinct conformational states, reconstructing the underlying free energy landscapes (see Figure S1), and identifying the most stable and long-lived conformations. Thus, the selected states for subsequent docking studies are not only structurally relevant, but also statistically and energetically significant (see Figure S1). In this analysis, two of the sequences, **Cdk4-2** and **Cdk4-4**, showed a promising tendency to adopt extended, marginally compact structures (Figure 2A). We also observed "folded-like" states of **Cdk4-2** and **Cdk4-4**, which had Root-Mean-Square Deviation (RMSD) values of as low as ~1 Å (see Figure S2), although transiently, when compared to the folded CDK4 structure. To ask whether **Cdk4-2** or **Cdk4-4** might adopt conformations commensurate with binding to Hsp70 or Hsp90, two representative structures from the disordered ensemble were docked to the substrate-binding domain of Hsp70 (SBD; PDB: 1YUW) or the client binding cleft in the Hsp90-Cdc37 complex (PDB: 5FWK). The overall orientation of the peptide was then compared to the pose of benchmark, bound client. These analyses supported the possible binding of the sequences to both chaperones in a way that resembles known client peptides (Figures 2B and 2C), with relatively low RMSD values of ~1.2 Å observed in some states (Figure S2). Taken together, we predict that **Cdk4-2** and **Cdk4-4** efficaciously mimic unfolded regions of CDK4 that might be capable of binding to the known client-interaction sites of both Hsp70 and Hsp90.

We note here that initial simulation results suggested that the **Cdk4-1** and **Cdk4-3** peptides have limited resemblance to the structures that are recognized by the two chaperones. Moreover, when synthesized and experimentally tested, these peptides showed limited solubility, such that **Cdk4-1** and **Ckd4-3** were not pursued further.

Table 1. Sequences and simulation times of peptide mimics of CDK4 unfolding regions

	Sequence	Simulation Length (microseconds)
Cdk4-1	**F**ATSRTDREGPN	24 μs
Cdk4-2	LPIST-GG-**F**QMALTPVV	24 μs
Cdk4-3	**F**-GVAEIGVGAYG	24 μs
Cdk4-4	GG-**F**QMALTPVV	24 μs

The table reports the names, the amino acid sequence, and the MD simulation lengths of the peptides designed.

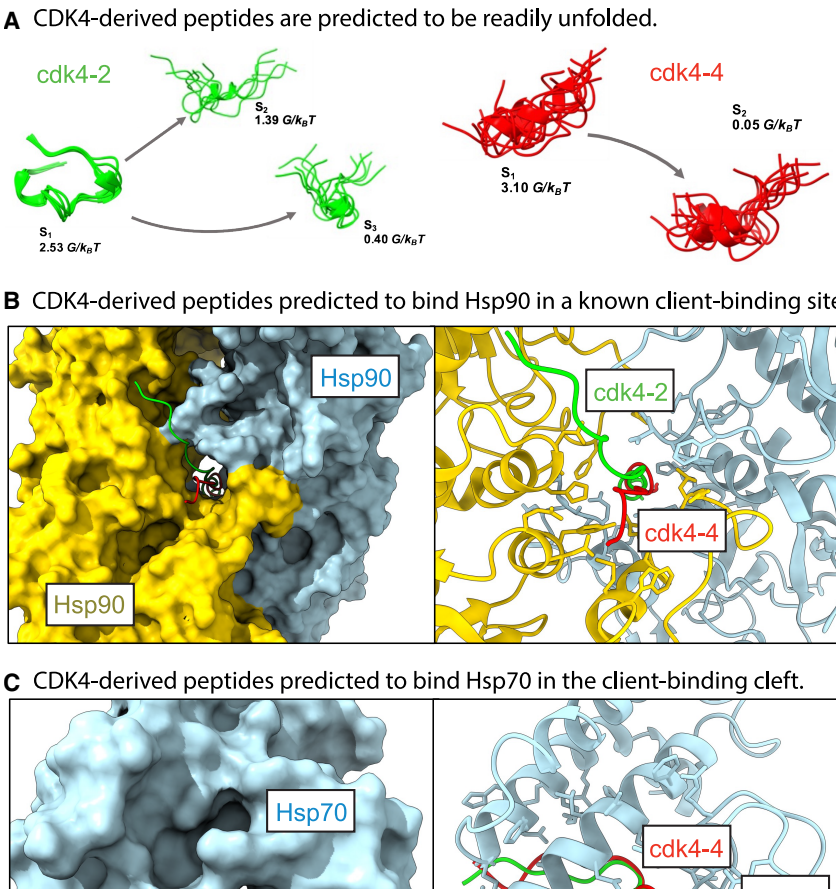

Figure 2. Conformational characterization and binding models of unfolding mimics

(A) Schematic representation of the 3 macrostates mapped by the Markov State Model (MSM) built on the 24 μs MD metatrajectory of **Cdk4-2** (green) or **Cdk4-4** (red) together with their respective free energies calculated by PyEMMA. The arrows interconnecting each pair of macrostates represent the kinetics of their interconversion, as determined by the mean first passage time method (MFPT). For each macrostate, the five most representative structures are shown.

(B) Models of the complexes formed by **Cdk4-2** (green) and **Cdk4-4** (red), with the client binding site of Hsp90. In the left panel, the Hsp90 surface is depicted with the two protomers colored gold and light blue. The right panel shows the Hsp90 residues interacting with **Cdk4-2** (green) and **Cdk4-4** (red).

(C) Models of the complexes formed by **Cdk4-2** (green) and **Cdk4-4** (red), with the substrate binding site (SBD) of Hsp70 (blue).

CDK4-derived peptides bind to Hsp70 and Hsp90 in cell lysates and cause apoptosis in kidney cancer cells

We first verified whether **Cdk4-2** and **Cdk4-4** could bind to Hsp70 and Hsp90 in cell lysates. Accordingly, we synthesized **Cdk4-2** and **Cdk4-4** peptides with a biotin moiety appended on the N-termini from a short linker (see STAR Methods) and used these probes in pulldown experiments from HEK293 cell lysates. In these experiments, we systematically increased the concentration of the probes added to lysates, performed pulldown experiments and then performed Western blots for Hsp70 and Hsp90 (see STAR Methods). We found that 0.1 μM of biotinylated **Cdk4-2** (**Bio-Cdk4-2**) pulled-down both Hsp70 and Hsp90 from lysate, while 1.0 μM of **Bio-Cdk4-4** only bound substantially to Hsp90 (Figure 3A). The identity of the bound Hsp70 and Hsp90 was further confirmed by mass spectrometry (Table S1; Figure S3A). These results suggest that **Cdk4-2** binds both Hsp70 and Hsp90, while **Cdk4-4** binds Hsp90.

Previous work has shown that CDK4 plays a prosurvival role in clear cell renal cell carcinoma (ccRCC) cells.[25,30] Therefore, we hypothesized that active peptides might limit CDK4 activity and induce apoptosis in these cells. First, we tested the permeability of our fluorescently labeled **Cdk4-2** and **Cdk4-4** peptides in the ccRCC 786-O cells. While many peptides are only weakly permeable,[31] this feature is relatively hard to predict and therefore, we tested it empirically for these specific peptides. Fortunately, in this case, we observed dose-dependent accumulation of diffuse fluorescence in 786-O cells after 24 h treatment (Figure 3B), consistent with at least partial peptide uptake and a dispersed localization in the cell. To determine if treatment with **Cdk4-2** or **Cdk4-4** impacts CDK4 activity, we treated 786-O cells with unlabeled **Cdk4-2** and **Cdk4-4** peptides for 24 h and assessed phosphorylation of the CDK4 substrate Retinoblastoma (Rb) at sites S807/S811 by Western blot. Consistent with diminished CDK4 activity, we observed a decrease in phosphorylated Rb in the presence of both peptides, but not **Cdk4-1** as a control (Figure 3C). Also, treatment with **Cdk4-2** or **Cdk4-4** led to an induction of apoptosis, as evident by cleavage of caspase-3 (Figures 3C, 3D, and S2B), consistent with the required role of CDK4 in these cells. Importantly, **Cdk4-2** and **Cdk-4** were also permeable in a normal kidney epithelium cell line, HK-2 (Figure 3E), but they did not induce caspase cleavage (Figures 3F and S2C). Given that **Cdk4-2** and **Cdk4-4** are not optimized for potency or permeability, we did not expect dramatic activity in these cell-based assays; yet, the results are encouraging and supportive of the idea that they might serve as a useful starting point for future development.

CDK4-derived peptides binding to Hsp90 and Cdc37

Motivated by the apparent binding of the peptides to chaperones in cell lysate, we moved to biophysical studies using purified proteins. In the initial experiments, we turned to solution state NMR.[32,33] Specifically, we used ^{19}F-T_2 filter experiments[34,35] to explore the interaction of **Cdk4-2** and **Cdk4-4** peptides with

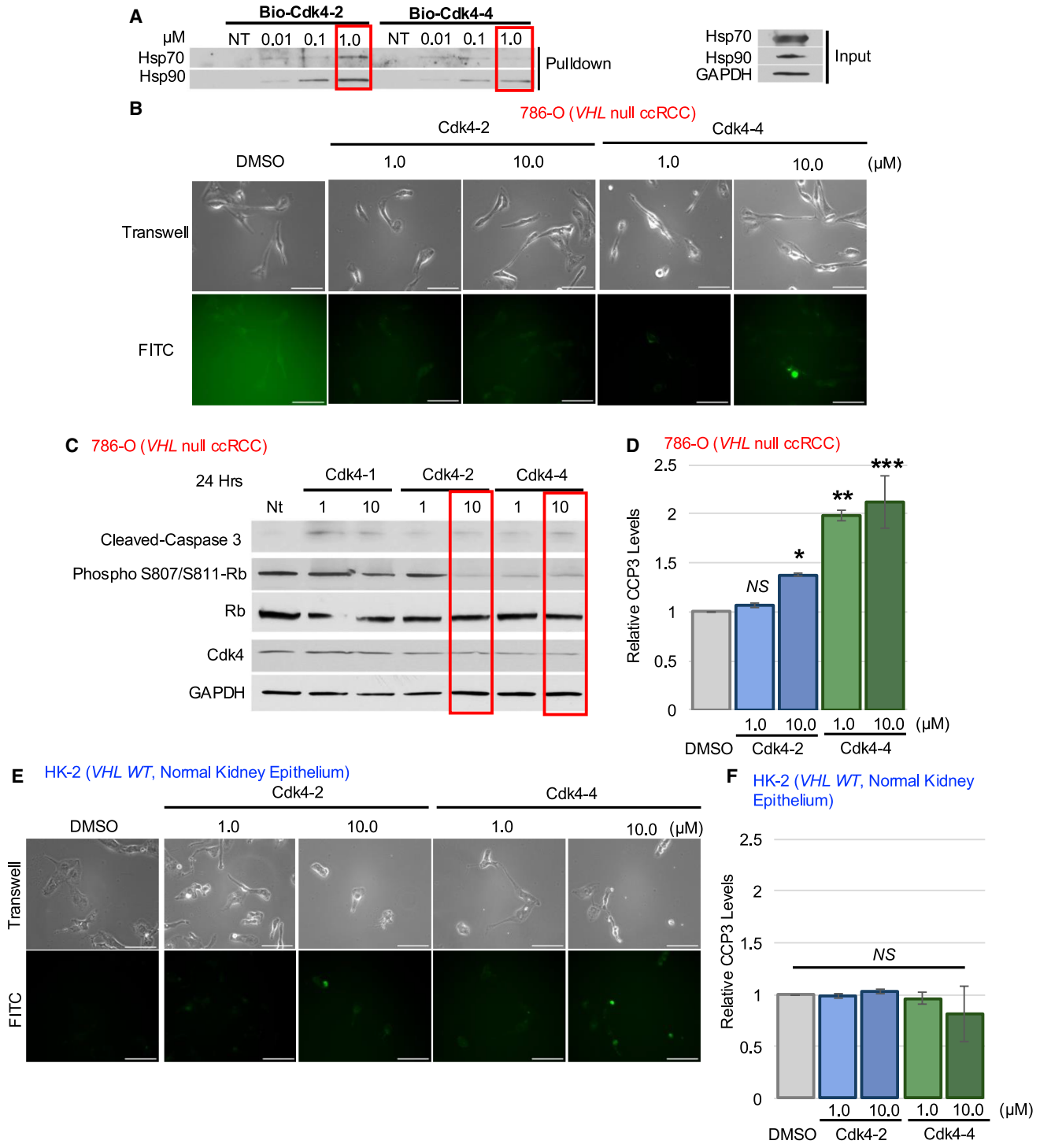

Figure 3. CDK4-derived peptides are partially membrane permeable and pro-apoptotic in clear cell renal cell carcinoma

(A) HEK293 cell lysates were incubated with biotinylated Cdk4-2 or Cdk4-4 peptides for 1 h prior to incubation with streptavidin-coated agarose beads. Pulldown of Hsp70 and Hsp90 was assessed by immunoblotting and mass spectrometry (see supplemental information).

(B) Representative microscopy images of ccRCC 786-O cells treated with indicated amounts of Cdk4-2 or Cdk4-4 FAM peptides for 24 h. Scale bar is 100 μm.

(C) 786-O cells were treated with CDK4 peptides for 24 h. DMSO was used as control (NT). Inhibition of CDK4 was assessed by phosphorylation of its substrate phospho S807/S811-retinoblastoma (Rb). Induction of apoptosis was evaluated by immunoblotting using cleaved caspase 3. GAPDH was used as a loading control. Results are representative of experiments performed three times.

(legend continued on next page)

purified, human Hsc70 (HSPA8), Hsp90 (HSP90AA) and Cdc37. Hsc70 is the constitutively expressed isoform of the human Hsp70 family member and we used it as a model target. The transverse relaxation rate, R_2 of ^{19}F is an extremely sensitive parameter for detecting binding events.[33,34] Especially at high magnetic field, R_2 is predominantly influenced by the large exchange contribution, arising from the difference in isotropic chemical shift (^{19}F δ) between the free (δ_f) and bound (δ_b) states, and the chemical shift anisotropy (CSA) of ^{19}F. These properties make ^{19}F NMR particularly well-suited for identifying even very weak binders, especially those in fast or fast-medium exchange with the target. In other words, the ^{19}F signal line broadens and becomes less intense when the peptide binds to its target, thus serving as a reliable indicator of binding interactions. To perform these experiments, we synthesized **Cdk4-2** and **Cdk4-4** variants with ^{19}F labels on the shared Phe residue (Tables S2 and S3). We then collected benchmark ^{19}F-NMR spectra of the two peptides at different concentrations (10, 50, and 100 μM) and different time points (just after preparation t_0 and after 48 h t_1) in the absence of protein to evaluate their solubility and stability under NMR conditions. Both fluorinated peptides showed excellent solubility and stability under these conditions (Figure S4). However, in initial experiments, we found that addition of either peptide to purified Hsc70 led to aggregation, so we were unable to use this approach to study binding to that chaperone (see below). Turning to Hsp90, we used ^{19}F T_2-filter experiments with **Cdk4-2** and **Cdk4-4**, and a randomly scrambled version of **Cdk4-2** (sequence**: Cdk4-2-scr**, PGQLMAISVGPTTL**F**V) as single peptides and in a mixture, with or without two different concentrations (10.0 μM and 4.0 μM) of Hsp90. At the highest Hsp90 concentration (10.0 μM), we observed binding. At the lower Hsp90 concentration (4.0 μM), no binding was observed for the scrambled peptide, while **Cdk4-2** and **Cdk4-4** still allowed the observation of a clear binding effect (Figure 4A). To confirm this interaction using a different experimental platform, we determined the binding affinities of **Cdk4-2** and **Cdk4-4** peptides to purified Hsp90 via microscale thermophoresis (MST) (Figure S5), revealing weak affinities of ∼90 μM. Thus, both **Cdk4-2** and **Cdk4-4** bound to Hsp90.

We next tested binding of the peptides to the co-chaperone Cdc37. As mentioned above, Cdc37 is known to recruit kinases to Hsp90; yet, the binding site(s) of this co-chaperone are not yet clear. We reasoned that Cdc37 might also have a tendency to bind unstable regions of clients, potentially allowing it to select appropriate clients for the Hsp90 system. Indeed, we found that the ^{19}F signals of both **Cdk4-2** and **Cdk4-4** peptides disappeared in the presence of 5 μM Cdc37 (Figure 4B; red), suggesting an interaction. We further explored this finding by conducting a dose–response experiment. Titrating the ^{19}F-peptides with increasing Cdc37 concentrations confirmed the binding of both peptides (Figure 4C). Importantly, when we replaced **Cdk4-2** with its scrambled version, no interaction was observed (Figure S6). Taken together, these results suggest that **Cdk4-2** and **Cdk4-4** peptides bind to both Hsp90 and Cdc37. **Cdk4-2**, which turned out to be the active lead in our studies (*vide infra*) was finally tested for its binding to Cdc37 via MST, confirming an affinity in the same micromolar range as for Hsp90 (Figure S5).

Cdk4-2 has a high affinity for Hsp70

Our pulldown experiment suggested that **Cdk4-2**, but not **Cdk4-4**, binds Hsp70 in cell lysates (Figure 3A). Because the NMR assay was not suitable for this system, we turned to a widely used fluorescence polarization (FP) assay[36] as an alternative. In this experiment, a fluorescent peptide (FAM-LVEAVY; termed the "tracer") is bound to a truncated substrate-binding domain (SBD) of human Hsc70 (HSPA8) and potential ligands are titrated into the system to calculate an inhibition constant (K_i). We first confirmed that an unlabeled, benchmark peptide, Ac-NRLLLTG. This peptide has been extensively used in previous studies as a high affinity model of Hsp70 substrates.[23,37–39] NRLLLTG recapitulates the physicochemical requirements for an unfolded client stretch to be recognized by the SBD of the chaperone and has the expected K_i value (∼0.4 μM; Figure 5A).[40–42] Then, we showed that **Cdk4-2**, but not **Cdk4-4**, bound with surprisingly tight affinity (K_i ∼0.1 μM) to the SBD of Hsc70. Because the FAM-LVEAVY tracer has an affinity of approximately 0.1 μM,[43–45] it cannot be used to accurately measure molecules with better affinity. Therefore, we synthesized a fluorescent analog of **Cdk4-2**, in which FAM is appended to the N-terminus with an Ahx linker, enabling more direct binding studies by FP. Indeed, titration of this probe with Hsc70 SBD confirmed a tight affinity (K_d = 0.029 ± 0.006 μM; Figure 5B), making this one of the strongest binding Hsp70 tracers yet reported. Using this tool, we performed competition studies with unlabeled NRLLLTG, **Cdk4-2** and **Cdk4-4**, showing that **Cdk4-2** and Ac-NRLLLTG displaced the tracer and that the control, **Cdk4-4**, was inactive (Figure 5C). It is important to note that the competitors were not able to fully displace the tracer (∼50% remaining at saturation), suggesting that the FAM fluorophore makes an expected contribution to the apparent affinity of this tracer. Regardless, combined with the NMR studies, these studies show that **Cdk4-2** binds to Hsp70, as well as Hsp90 and Cdc37.

Identification the minimal CDK4-derived peptide for Hsp70 binding

We were initially surprised that **Cdk4-2**, but not **Cdk4-4**, binds to Hsc70, because the sequence of **Cdk4-4** is subset of the longer **Cdk4-2** peptide (see Table 1). To better understand this result, we systematically truncated **Cdk4-2** from both ends to reveal

(D) Quantification of Western blot bands from panel C. Densitometry was performed using Photoshop v.23.5.1. Bars represent the mean signal intensity of cleaved caspase 3 (CCP3):GAPDH for each treatment relative to that of DMSO for three independent measurements. Tukey's multiple comparisons test was used to determine statistical significance compared to DMSO (NS = p value >0.05, *p < 0.05, **p < 0.005, ***p < 0.0005). The error bars are standard deviation of three measurements.
(E) Representative microscopy images of HK-2 normal kidney epithelium cells treated with indicated amounts of Cdk4-2 and Cdk4-4 FAM peptides for 4 h. Scale bar is 100 μm.
(F) HK-2 cells were treated with Cdk4 peptides or DMSO for 24 h. Apoptosis was evaluated by immunoblotting using CCP3 and GAPDH was used as a loading control. Densitometry was performed using Photoshop v.23.5.1 to quantify Western blot band signal intensity. Bars represent the mean signal intensity values of CCP3:GAPDH for each treatment relative to that of DMSO for three independent measurements. Tukey's multiple comparisons test was used to determine statistical significance compared to DMSO. The error bars are standard deviation of three measurements.

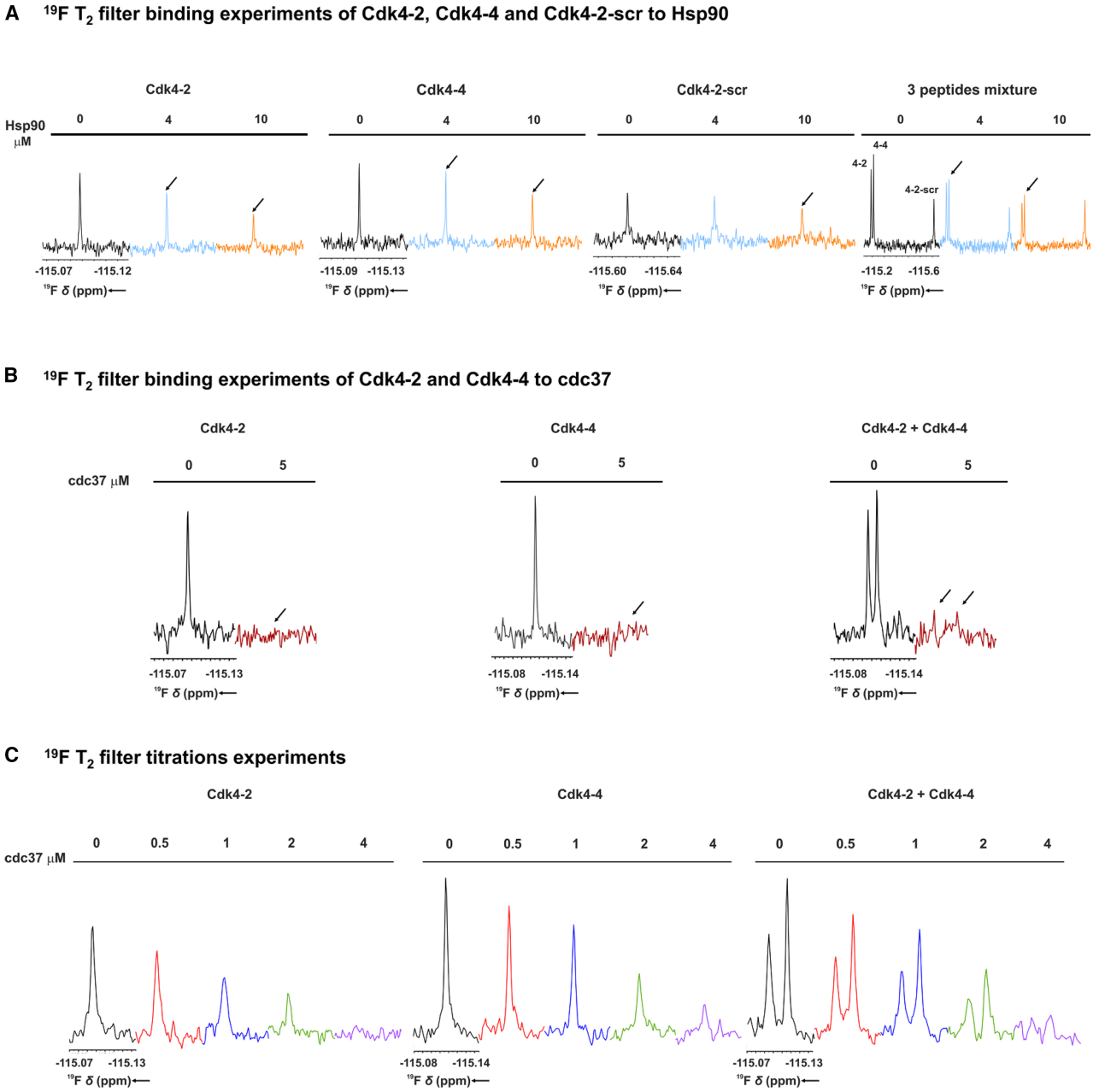

Figure 4. Biophysical characterization of CDK4-derived peptides binding to Hsp90 and Cdc37

(A) ^{19}F T_2 filter spectra of peptides **Cdk4-2**, **Cdk4-4**, the scrambled control **Cdk4-2-scr** (10 μM), and their mixture recorded in the absence (black) and in presence of Hsp90 (4 μM light blue, 10 μM orange). Arrows indicate binding events.

(B) ^{19}F T_2 filter spectra of the two peptides **Cdk4-2** and **Cdk4-4** (20 μM) and their mixture in the absence (black) and in presence (dark red) of Cdc37 (5 μM). Arrows indicate binding events.

(C) Titration series of ^{19}F T_2 filter NMR spectra for peptides **Cdk4-2** and **Cdk4-4** recorded in the absence (black) and in presence of increasing concentrations (red, blue, green, violet) of Cdc37. Protein concentrations are indicated above each spectrum.

the minimal sequence required for binding to the SBD of Hsc70. Using competitive FP experiments, we found that the first six residues of **Cdk4-2** could be removed without a substantial loss of affinity (Figure 6A). This indicates that **Cdk4-4** does not bind because this peptide lacks the seemingly required Thr residue. We next systematically removed residues from the C-terminus, revealing that the last three residues are dispensable (Figure 6B). The resulting minimal pharmacophore, Ac-TGGFQMALT, retained an affinity (K_i = 0.12 ± 0.01 μM) that was approximately similar to the full length **Cdk4-2** (K_i = 0.1 ± 0.01 μM) and at least 5-fold better than the previous benchmark peptide, Ac-NRLLLTG (K_i 0.56 ± 0.05 μM). Furthermore, the

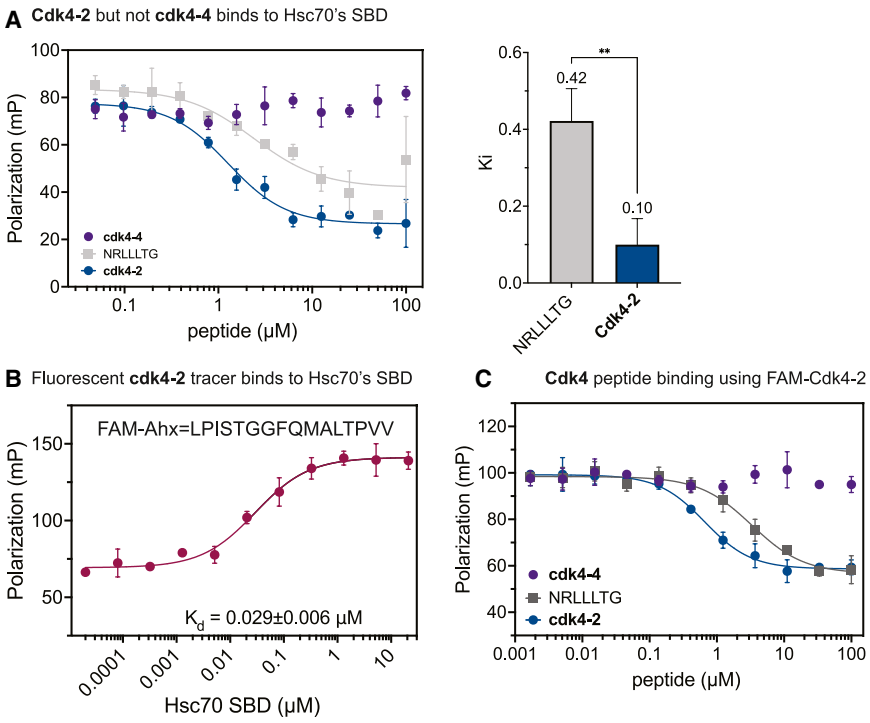

Figure 5. Cdk4-2 peptide binds tightly to Hsc70 SBD *in vitro*

(A) In competition FP experiments, Cdk4-2 binds Hsc70 SBD (K_i = 0.09 ± 0.06 μM), while Cdk4-4 does not (K_i > 100 μM). Cdk4-2 binds even tighter than the positive control, Ac-NRLLLTG (K_i = 0.42 ± 0.08 μm M; ***p* value 0.0075).

(B) Saturation binding curve of a Cdk4-2 tracer (1 nM; FAM-Ahx-LPISTGGFQMALTPVV-OH) to Hsc70 SBD (Kd = 0.029 ± 0.006 μM).

(C) In competition FP experiments using the Cdk4-2 tracer, the K_i of unlabeled Cdk4-2 was determined to be 0.04 ± 0.01 μM. Note that the competition signal does not go to zero, indicating a contribution of non-specific binding. In all of the FP experiments, the results are the average of experiments performed in independent triplicates and error bars represent standard deviation (SD).

minimal pharmacophore retained the ability to inhibit CDK4 activity and induce apoptosis in 786-O ccRCC cells, as evidenced by reduced Rb phosphorylation and elevated levels of cleaved caspase-3, cleaved caspase-8, and cleaved PARP (Figure 6C).

Alanine scanning reveals potentially important contacts between Cdk4-2 and Hsp70

The Ac-TGGFQMALT sequence is one of the tightest reported Hsc70 ligands. Thus, we next wanted to perform an alanine scan to understand the binding contributions of each residue. Strikingly, most of the alanine substitutions had only a modest impact on apparent affinity (Figure 7A), but mutation of the Met or Leu residues significantly (>10-fold) weakened binding (Ki ~1 to 1.7 μM). To build a structural basis for interpreting this result, we docked the minimal peptide to Hsc70 SBD (PDB: 1YUW). Then, from the best docked pose, we performed eight independent simulations, each 1 microsecond long for a total of 8 microseconds of sampling. We clustered the resulting combined trajectory and explored the three main representatives. From this analysis, we first noticed that the overall position of the peptide (Figure 7B) was largely consistent with that of other Hsp70-bound ligands,[41,46,47] with the peptide backbone making multiple H-bond interactions in a narrow cleft. In addition, a few specific side chain contacts were suggested; for example, the Phe side chain of TGGFQMALT appeared to be buried relatively deeply in the cleft, establishing a local contact network. Next, we focused on the interactions with the Met and Leu sidechains, which the alanine scan suggested are the most important. Indeed, the Met residue was buried deep into a pocket formed from Phe428, Gln426 and Thr411 on the "bottom" and Ser537 and Glu534 on the "top" (Figure 7C). Intriguingly, the sulfur of the Met was placed within 5 Å of the Phe428 residue, such that favorable stacking seemed possible. The Leu sidechain of Ac-TGGFQMALT was positioned at the exit from the cleft, projecting into a small pocket formed from Tyr545, Gln612 and Arg596, with especially close packing with aromatic ring of the Tyr545 (Figure 7D). Side chain interactions are relatively sparse in the structures of other ligands bound to Hsp70 client-binding cleft,[43,48,49] thus, we propose, based on the docking and alanine scan, that these contacts might contribute to the unusually tight affinity of **Cdk4-2** peptide.

DISCUSSION

In this study, we report the discovery of **Cdk4-2**, a multi-targeted inhibitor of the Hsp70/Hsp90 chaperone machinery. The design of this peptide was inspired by observations that chaperones and co-chaperones normally collaborate in binding to clients[17] and that they generally tend to prefer disordered sites.[23] Using computational methods, we selected four peptides predicted to be unstable and prone to unfolding in the native structure of the model client, CDK4. Then, using experimental methods, we show that one of these peptides, **Cdk4-2**, binds Hsp70, Hsp90, and the kinase-selective co-chaperone, Cdc37. This compound was partially membrane permeable and even had activity in renal cell carcinoma cells, suggesting that **Cdk4-2** may compete with multiple steps in the native activation mechanism of CDK4. Consistent with this idea, found that treatment of ccRCC cells with **Cdk4-2** lowers levels of phospho-S807/S811-Rb and induces caspase-3 cleavage. However, we want to stress that more work is needed to develop the potency, selectivity and drug-like properties of **Cdk4-2**. Yet, these results suggest that **Cdk4-2** is the first, fully rationally designed, multi-targeting chaperone ligand and we predict that it could be a promising starting point for therapeutic development.

There is great interest in predicting the binding sites of molecular chaperones. There are multiple tools available for predicting the binding sites of Hsp70 within a client primary sequence.[50,51] However, these algorithms are based on limited experimental studies and none of them were able to identify the **Cdk4-2** sequence as a putative Hsc70-binding site. Moreover, there are no equivalent

A N-terminal truncation of **Cdk4-2** reveal necessary amino acids for binding to Hsc70's SBD

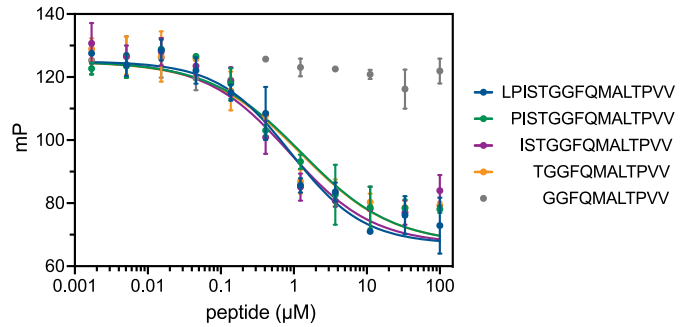

Peptide	Ki (μM)
LPISTGGFQMALTPVV	0.10 ± 0.02
PISTGGFQMALTPVV	0.15 ± 0.03
ISTGGFQMALTPVV	0.09 ± 0.03
TGGFQMALTPVV	0.14 ± 0.03
GGFQMALTPVV	ns

B C-terminal truncation shows that the three two amino acids of **Cdk4-2** are not needed for binding Hsc70's SBD

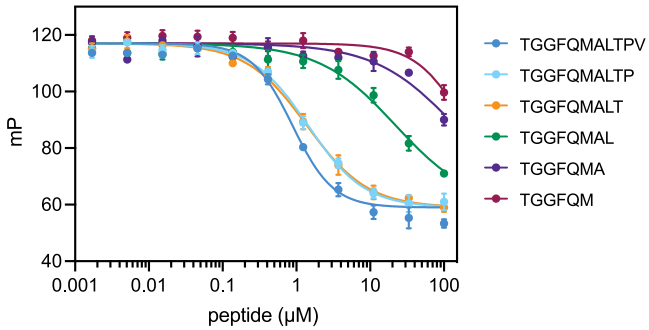

Peptide	Ki (μM)
TGGFQMALTPV	0.056 ± 0.007
TGGFQMALTP	0.11 ± 0.01
TGGFQMALT	0.10 ± 0.01
TGGFQMAL	2.0 ± 0.2
TAGFQMA	ns
TGAFQM	ns

C Minimal Cdk4 peptide inhibits cdk4 activity and induces apoptosis in 786-O cells.

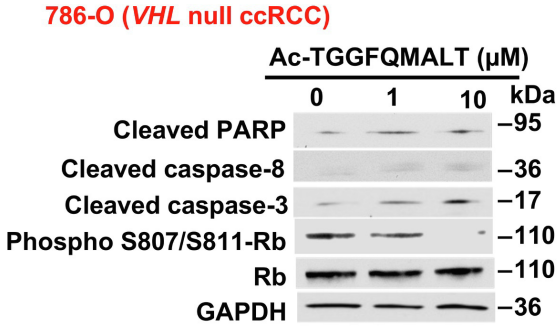

Figure 6. Truncation of the N- and C-termini reveals the minimal pharmacophore for cdk4-2 binding to Hsc70 SBD

(A) Systematic truncation of residues at the N-terminus points to a dramatic weakening of affinity upon removal of a Thr residue. Competition FP experiments were performed with the **Cdk4-2** tracer (1 nM).

(B) Systematic truncation of the C-terminus shows that the last three residues are not required for activity. Competition FP experiments were performed with the **Cdk4-2** tracer (1 nM). All results are shown as the average of three independent experiments performed in triplicate each. The error bars represent SD.

(C) 786-O cells were treated with the indicated amounts of the minimal pharmacophore peptide for 24 h. Apoptosis was evaluated by immunoblotting for cleaved caspase-3, cleaved caspase-8, and cleaved PARP. Inhibition of CDK4 was assessed by phosphorylation of its substrate phospho-S807/S811-retinoblastoma (Rb). GAPDH was used as a loading control.

tools for predicting the binding site of Hsp90 or Cdc37. Rather, we envisioned a different way to think about this problem. Specifically, we designed a computational approach that is based on the idea that chaperones might be evolutionarily tuned to identify sequences of a client that are prone to be unstable and/or undergo unfolding, perhaps less confined by the exact sequence. Here, we characterized the distribution of CDK4 stabilization energy in the native state and then analyzed the nonbonded interactions that each residue establishes with all other residues within the native state ensemble. This strategy is designed to separate the strong pair-interaction patterns that define the folding core (i.e., those that determine the overall 3D structure) from those weak

A Alanine scanning reveals key residues involved in cdk4-2 binding to Hsc70

Peptide	Ki (μM)
NRLLLTG	0.56 ± 0.05
LPISTGGFQMALTPVV	0.10 ± 0.01
TGGFQMALT	0.12 ± 0.01
AGGFQMALT	0.11 ± 0.01
T**A**GFQMALT	0.36 ± 0.05
TG**A**FQMALT	0.37 ± 0.05
TGG**A**QMALT	0.26 ± 0.03
TGGF**A**MALT	0.17 ± 0.02
TGGFQ**A**ALT	1.05 ± 0.07
TGGFQMA**A**T	1.7 ± 0.1
TGGFQMAL**A**	0.22 ± 0.02

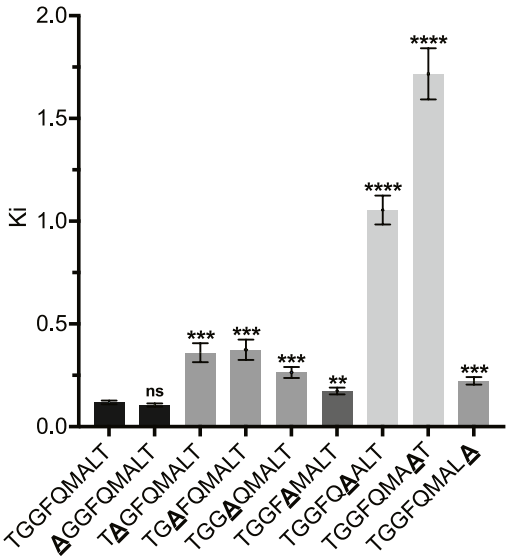

B Docking of the minimal cdk4-2 peptide to Hsc70 suggests key molecular contacts

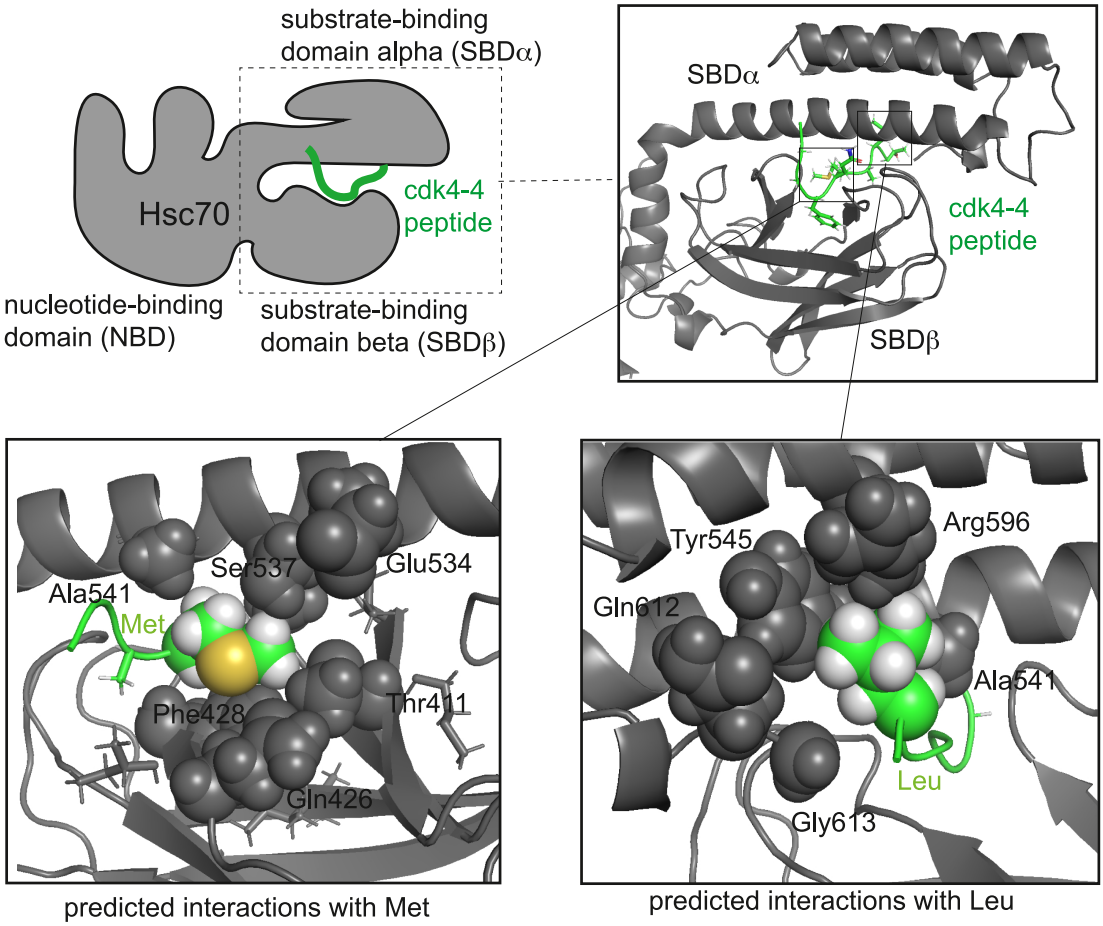

Figure 7. Alanine scanning and docking suggest that key contributions of the Met and Leu residues within the minimal cdk4-2 peptide

(A) Competition FP experiments performed using the Cdk4-2 tracer. Results are shown as the average of at least three experiments performed in triplicate. Error bars are SD. ns = *p* value >0.05. ***p* value <0.01. ****p* value <0.005. *****p* value <0.001.

(B) Docking and molecular dynamics simulations suggest that Met and Leu side chains interact with side pockets Hsc70 SBD. See text for details.

pair-interaction patterns that we predict would constitute unstable substructures. Specifically, we reasoned that the weakly paired regions might be poised to populate alternative conformations and, moreover, be more prone to local and global unfolding. This approach seemed promising to try because Hsp70 tends to have tighter binding to disordered regions, based on the topology of its client-binding cleft,[23,47,52] and recent structures of Hsp90 bound to partially folded clients have suggested that it seeks out similarly elongated substructures that are adjacent to folded domains.[26,27,53–55] In other words, the Hsp70/Hsp90 system appears to associate with substrates in which parts of the domains can be already in their native conformation. On this basis, our working hypothesis is that unstable regions of folded clients (a concept reminiscent of local frustration[56]) could represent sites preferred by Hsp70, Hsp90 and potentially other chaperones and co-chaperones. This computational approach might supplement experimental methods, such as phage display, proteomics and peptide microarrays, which aim to identify and describe chaperone-binding peptides.

One of the unanticipated findings in this work is that **Cdk4-2** and **Cdk4-4** bind to Cdc37. This co-chaperone is dedicated to recognizing and sorting kinases,[19,26,57–59] but the direct binding sites of Cdc37 are under-explored. Our results suggest that Cdc37 may, in part, recognize short, disordered stretches within CDK4, akin to what is typically thought for the main chaperones. Importantly, a scrambled version of **Cdk4-2** did not bind, indicating that client sorting by this co-chaperone might involve a degree of sequence selectivity (and not just physicochemical properties), corroborating results by the Gelis group using NMR.[19,59] Thus, it seems possible that Cdc37 binds to specific sequences in partially unfolded CDK4 during its recruitment of Hsp90 into chaperone complexes. Because the same peptides bound Hsp90 (see Figure 2), it is also possible that Hsp90 could displace Cdc37 during complex maturation and assembly, but this idea remains to be tested.

At this point, the different affinities demonstrated by **Cdk4-2** for Hsp90/Cdc37 versus Hsp70 raise interesting mechanistic questions. From the general point of view,[60] one key characteristic of the Hsp90 chaperone mechanisms is that binding to clients is typically weak. This weak affinity allows chaperone–client interactions to be readily outcompeted by the stronger, intramolecular contacts that form in folded state of the client.[61] In other words, it is thought that the weak affinity of these interactions provides directionality to the folding process, guiding it towards the active state of the client.[62] Weak interactions with clients are also observed for co-chaperones: in the case of Cdc37, weak interactions can be instrumental for the co-chaperone to rapidly sort the client and select it for engagement in the complex with Hsp90 or release it, as suggested by the models proposed by Gelis and coworkers.[19,59]

In this picture, Hsp90 binds to proteins late in the folding process, specifically recognizing exposed hydrophobic residues and/or disordered regions spanning a rather extended surface area.[42] Such features areshared by a number of proteins, and this set of features is clearly captured by the **Cdk4-2** peptide.[26,27,63–65]

Finally, in Hsp90 complexes, high affinity interactions would stall the final stages of client maturation which might facilitate the dynamic exchange of proteins among different complexes.[53–55]

In contrast to Hsp90, Hsp70 binds earlier in the folding reaction, capturing largely unfolded and disordered stretches that need to be bound with high affinity to avoid aggregation.[40–42] In this framework, Hsp70 generally shows a relatively tight affinity for short stretches containing typically three or more large hydrophobic or aromatic residues.[42,66] Such stretches may be hidden inside both folded states and late folding intermediates,[67] and proteins thus need to (partially) unfold to expose Hsp70 binding sites, as confirmed for instance by the Hsp70–GR contacts in the GR-maturation complex.[55]

The above discussed model is consistent with Hsp70 guarding integral elements of the unfolding states of proteins, protecting them from aggregation, which requires that the advancement of the folding reaction is somewhat stalled. Hsp90, in contrast, binds at a later, near native or native state, which would require a more dynamic exchange of almost folded clients among different complexes.[40–42]

Cdk4-2 appears to recapitulate the physicochemical properties of an unfolded protein element. The binding affinities of the peptide for Hsp70 and Hsp90/Cdc37 reverberate the way these machines interact with their substrates. Additionally, it is worth noting here that **Biotin-Cdk4-2** pulled down both Hsp70 and Hsp90 from cell lysate suggesting the affinity is strong enough to have a combinatorial impact in cells.

As a caveat, it is important to note that our experiments are mostly conducted *in vitro* on isolated molecules, and may provide a partial view of what may be happening in the intricate inside of the cell. However, at least from a mechanistic point of view, our design appears to capture the minimal necessary elements for a sequence to be engaged by the chaperone machinery.

In conclusion, we hypothesize that **Cdk4-2** mimics the unfolded state of CDK4 and interferes with multiple, weak protein-protein interactions in the chaperone machinery. This variation on the concept of "dual targeting compounds" might allow a single molecule/peptide to interact with multiple parts of the chaperone network. Even if some of these inhibitory contacts are weak, the amalgam might contribute to slowed CDK4 maturation. It remains to be seen whether **Cdk4-2** can be optimized as a research probe or therapeutic, but it appears to be a first-in-class Hsp70 and Hsp90 multitargeting agent able to perturb the activities of multiprotein chaperone complexes whose functions are required for cancer development. Interestingly, the simulated binding modes and the modeling experiments show that the peptide-chaperone interactions are governed mainly by the side-chain contacts, while peptide backbone elements are not involved in key contacts. This observation opens the way to the engineering of stable derivatives in the form of peptidomimetics to improve the profiles of these reagents in future studies.

We anticipate that this multi-targeting strategy could have benefits in leveraging chaperone networks in the development of new therapeutics against cancer and other diseases where chaperone-network malfunctions are central.[68]

RESOURCE AVAILABILITY

Lead contact

Further information and requests for resources and reagents should be directed to and will be fulfilled by the Lead Contact, Dr. Giorgio Colombo (g.colombo@unipv.it).

Materials availability

All unique reagents generated in this study are available from the lead contact with a completed Materials Transfer Agreement.

Data and code availability

- Code used in this work is publicly available as of the date of publication from https://github.com/colombolab, and publicly available as of the date of publication.
- Docking data are deposited under https://doi.org/10.5281/zenodo.16088778 for Hsp70; and under https://doi.org/10.5281/zenodo.16089216 for Hsp90, and publicly available as of the date of publication.
- MD input files are deposited under https://doi.org/10.5281/zenodo.16089270 for the simulations of short sequences; https://doi.org/10.5281/zenodo.16089407 for the simulations of Hsp70-short peptide complexes, and publicly available as of the date of publication.
- Any additional information required to reanalyze the data reported in this paper is available from the lead contact upon request.

ACKNOWLEDGMENTS

This work was supported by grants from the US National Institutes of Health (NS059690 to J.E.G. and R35GM139584 to M.M.). Giorgio Colombo acknowledges funding from Fondazione AIRC (Associazione Italiana Ricerca Sul Cancro) under IG 2022 - ID. 27139, from PRIN (grant 20209KYCH9), from IMMUNO-HUB, T4-CN-02, from the Ministero della Salute, and from Research Programme CN00000013 "National Centre for HPC, Big Data and Quantum Computing". G.C. would like to acknowledge ASINO Foundation for support. We would like to thank Elhan F. Ahanin for her technical support.

AUTHOR CONTRIBUTIONS

L.T., M.C., J.A.H., S.J.C., S.J.B., S.A.S., F.D., and M.V., performed research, wrote manuscript; F.M., J.H., A.M., E.F., V.P., L.A.W., M.R.W., G.L., T.B., A.P., C.P., D.B., A.C., C.A., and M.L., performed research. S.G. and G.B., performed research, wrote manuscript, conceptualized technical parts, wrote revisions; J.E.G., M.M., and G.C., conceived the work, conceptualized the work, secured funding, coordinated research, wrote manuscript and revisions.

DECLARATION OF INTERESTS

The authors declare no competing interests.

STAR★METHODS

Detailed methods are provided in the online version of this paper and include the following:

- KEY RESOURCES TABLE
- EXPERIMENTAL MODEL AND STUDY PARTICIPANT DETAILS
  - Cell lines
- METHOD DETAILS
  - Computational methods
  - Experimental details
  - Peptide synthesis: General procedures
- QUANTIFICATION AND STATISTICAL ANALYSIS

SUPPLEMENTAL INFORMATION

Supplemental information can be found online at https://doi.org/10.1016/j.str.2025.07.021.

Received: February 28, 2025
Revised: July 2, 2025
Accepted: July 30, 2025
Published: August 25, 2025

REFERENCES

1. Hartl, F.U., Bracher, A., and Hayer-Hartl, M. (2011). Molecular chaperones in protein folding and proteostasis. Nature *475*, 324–332.
2. Trepel, J., Mollapour, M., Giaccone, G., and Neckers, L. (2010). Targeting the dynamic Hsp90 complex in cancer. Nat. Rev. Cancer *10*, 537–549.
3. Albakova, Z., Mangasarova, Y., Albakov, A., and Gorenkova, L. (2022). HSP70 and HSP90 in Cancer: Cytosolic, Endoplasmic Reticulum and Mitochondrial Chaperones of Tumorigenesis. Front. Oncol. *12*, 829520.
4. Yang, S., Xiao, H., and Cao, L. (2021). Recent advances in heat shock proteins in cancer diagnosis, prognosis, metabolism and treatment. Biomed. Pharmacother. *142*, 112074. https://doi.org/10.1016/j.biopha.2021.112074.
5. Park, H.-K., Yoon, N.G., Lee, J.-E., Hu, S., Yoon, S., Kim, S.Y., Hong, J.-H., Nam, D., Chae, Y.C., Park, J.B., and Kang, B.H. (2020). Unleashing the full potential of Hsp90 inhibitors as cancer therapeutics through simultaneous inactivation of Hsp90, Grp94, and TRAP1. Exp. Mol. Med. *52*, 79–91. https://doi.org/10.1038/s12276-019-0360-x.
6. Gestwicki, J.E., and Shao, H. (2019). Inhibitors and chemical probes for molecular chaperone networks. J. Biol. Chem. *294*, 2151–2161. https://doi.org/10.1074/jbc.TM118.002813.
7. Shkedi, A., Adkisson, M., Schroeder, A., Eckalbar, W.L., Kuo, S.-Y., Neckers, L., and Gestwicki, J.E. (2021). Inhibitor Combinations Reveal Wiring of the Proteostasis Network in Prostate Cancer Cells. J. Med. Chem. *64*, 14809–14821. https://doi.org/10.1021/acs.jmedchem.1c01342.
8. Kurokawa, Y., Honma, Y., Sawaki, A., Naito, Y., Iwagami, S., Komatsu, Y., Takahashi, T., Nishida, T., and Doi, T. (2022). Pimitespib in patients with advanced gastrointestinal stromal tumor (CHAPTER-GIST-301): a randomized, double-blind, placebo-controlled phase III trial. Ann. Oncol. *33*, 959–967. https://doi.org/10.1016/j.annonc.2022.05.518.
9. Neckers, L., and Workman, P. (2012). Hsp90 Molecular Chaperone inhibitors: are we there yet? Clin. Cancer Res. *18*, 64–76.
10. Neckers, L., Blagg, B., Haystead, T., Trepel, J.B., Whitesell, L., and Picard, D. (2018). Methods to validate Hsp90 inhibitor specificity, to identify off-target effects, and to rethink approaches for further clinical development. Cell Stress Chaperones *23*, 467–482. https://doi.org/10.1007/s12192-018-0877-2.
11. Rastogi, S., Joshi, A., Sato, N., Lee, S., Lee, M.-J., Trepel, J.B., and Neckers, L. (2024). An update on the status of HSP90 inhibitors in cancer clinical trials. Cell Stress Chaperones *29*, 519–539. https://doi.org/10.1016/j.cstres.2024.05.005.
12. Workman, P. (2020). Reflections and Outlook on Targeting HSP90, HSP70 and HSF1 in Cancer: A Personal Perspective. In HSF1 and Molecular Chaperones in Biology and Cancer (Springer), pp. 163–179.
13. Raghavendra, N.M., Pingili, D., Kadasi, S., Mettu, A., and Prasad, S.V.U.M. (2018). Dual or multi-targeting inhibitors: The next generation anticancer agents. Eur. J. Med. Chem. *143*, 1277–1300. https://doi.org/10.1016/j.ejmech.2017.10.021.
14. Genest, O., Wickner, S., and Doyle, S.M. (2019). Hsp90 and Hsp70 chaperones: Collaborators in protein remodeling. J. Biol. Chem. *294*, 2109–2120. https://doi.org/10.1074/jbc.REV118.002806.
15. Pearl, L.H. (2005). Hsp90 and Cdc37 – a chaperone cancer conspiracy. Curr. Opin. Genet. Dev. *15*, 55–61. https://doi.org/10.1016/j.gde.2004.12.011.
16. Schopf, F.H., Biebl, M.M., and Buchner, J. (2017). The HSP90 chaperone machinery. Nat. Rev. Mol. Cell Biol. *18*, 345–360. https://doi.org/10.1038/nrm.2017.20.
17. Pratt, W.B., and Toft, D.O. (1997). Steroid receptor interactions with heat shock protein and immunophilin chaperones. Endocr. Rev. *18*, 306–360.
18. Polier, S., Samant, R.S., Clarke, P.A., Workman, P., Prodromou, C., and Pearl, L.H. (2013). ATP-competitive inhibitors block protein kinase recruitment to the Hsp90-Cdc37 system. Nat. Chem. Biol. *9*, 307–312. https://doi.org/10.1038/nchembio.1212.
19. Keramisanou, D., Aboalroub, A., Zhang, Z., Liu, W., Marshall, D., Diviney, A., Larsen, R.W., Landgraf, R., and Gelis, I. (2016). Molecular Mechanism of Protein Kinase Recognition and Sorting by the Hsp90 Kinome-Specific

Cochaperone Cdc37. Mol. Cell *62*, 260–271. https://doi.org/10.1016/j.molcel.2016.04.005.

20. Banerjee, M., Hatial, I., Keegan, B.M., and Blagg, B.S.J. (2021). Assay design and development strategies for finding Hsp90 inhibitors and their role in human diseases. Pharmacol. Ther. *221*, 107747. https://doi.org/10.1016/j.pharmthera.2020.107747.
21. Marchetti, F., Capelli, R., Rizzato, F., Laio, A., and Colombo, G. (2019). The Subtle Trade-Off between Evolutionary and Energetic Constraints in Protein-Protein Interactions. J. Phys. Chem. Lett. *10*, 1489–1497.
22. Paladino, A., Woodford, M.R., Backe, S.J., Sager, R.A., Kancherla, P., Daneshvar, M.A., Chen, V.Z., Bourboulia, D., Ahanin, E.F., Prodromou, C., et al. (2020). Chemical Perturbation of Oncogenic Protein Folding: from the Prediction of Locally Unstable Structures to the Design of Disruptors of Hsp90–Client Interactions. Chemistry *26*, 9459–9465. https://doi.org/10.1002/chem.202000615.
23. Clerico, E.M., Tilitsky, J.M., Meng, W., and Gierasch, L.M. (2015). How Hsp70 Molecular Machines Interact with Their Substrates to Mediate Diverse Physiological Functions. J. Mol. Biol. *427*, 1575–1588. https://doi.org/10.1016/j.jmb.2015.02.004.
24. Romero-Pozuelo, J., Figlia, G., Kaya, O., Martin-Villalba, A., and Teleman, A.A. (2020). Cdk4 and Cdk6 Couple the Cell-Cycle Machinery to Cell Growth via mTORC1. Cell Rep. *31*, 107504. https://doi.org/10.1016/j.celrep.2020.03.068.
25. Sager, R.A., Backe, S.J., Ahanin, E., Smith, G., Nsouli, I., Woodford, M.R., Bratslavsky, G., Bourboulia, D., and Mollapour, M. (2022). Therapeutic potential of CDK4/6 inhibitors in renal cell carcinoma. Nat. Rev. Urol. *19*, 305–320. https://doi.org/10.1038/s41585-022-00571-8.
26. Verba, K.A., Wang, R.Y.R., Arakawa, A., Liu, Y., Shirouzu, M., Yokoyama, S., and Agard, D.A. (2016). Atomic structure of Hsp90-Cdc37-Cdk4 reveals that Hsp90 traps and stabilizes an unfolded kinase. Science *352*, 1542–1547.
27. Verba, K.A., and Agard, D.A. (2017). How Hsp90 and Cdc37 Lubricate Kinase Molecular Switches. Trends Biochem. Sci. *42*, 799–811. https://doi.org/10.1016/j.tibs.2017.07.002.
28. Paladino, A., Marchetti, F., Ponzoni, L., and Colombo, G. (2018). The Interplay between Structural Stability and Plasticity Determines Mutation Profiles and Chaperone Dependence in Protein Kinases. J. Chem. Theory Comput. *14*, 1059–1070. https://doi.org/10.1021/acs.jctc.7b00997.
29. Peri, C., Gagni, P., Combi, F., Gori, A., Chiari, M., Longhi, R., Cretich, M., and Colombo, G. (2013). Rational epitope design for protein targeting. ACS Chem. Biol. *8*, 397–404.
30. Shen, C., and Kaelin, W.G. (2013). The VHL/HIF axis in clear cell renal carcinoma. Semin. Cancer Biol. *23*, 18–25. https://doi.org/10.1016/j.semcancer.2012.06.001.
31. Tan, X., Liu, Q., Fang, Y., Zhu, Y., Chen, F., Zeng, W., Ouyang, D., and Dong, J. (2024). Predicting Peptide Permeability Across Diverse Barriers: A Systematic Investigation. Mol. Pharm. *21*, 4116–4127. https://doi.org/10.1021/acs.molpharmaceut.4c00478.
32. Dalvit, C., and Vulpetti, A. (2019). Ligand-based Fluorine NMR Screening: Principles and Applications in Drug Discovery Projects. J. Med. Chem. *62*, 2218–2244.
33. Buchholz, C.R., and Pomerantz, W.C.K. (2021). 19F NMR viewed through two different lenses: ligand-observed and protein-observed 19F NMR applications for fragment-based drug discovery. RSC Chem. Biol. *2*, 1312–1330. https://doi.org/10.1039/D1CB00085C.
34. Dalvit, C., Flocco, M., Veronesi, M., and Stockman, B.J. (2002). Fluorine-NMR Competition Binding Experiment for High-Throughput Screening of Large Compound Mixtures. Comb. Chem. HTS *5*, 605–611.
35. Dalvit, C., Fagerness, P.E., Hadden, D.T.A., Sarver, R.W., and Stockman, B.J. (2003). Fluorine-NMR Experiments for High-Throughput Screening: Theoretical Aspects, Practical Considerations, and Range of Applicability. J. Am. Chem. Soc. *125*, 7696–7703. https://doi.org/10.1021/ja034646d.
36. Ricci, L., and Williams, K.P. (2008). Development of Fluorescence Polarization Assays for the Molecular Chaperone Hsp70 Family Members: Hsp72 and DnaK. Curr. Chem. Genomics *2*, 90–95.
37. Stevens, S.Y., Cai, S., Pellecchia, M., and Zuiderweg, E.R.P. (2003). The solution structure of the bacterial HSP70 chaperone protein domain DnaK(393–507) in complex with the peptide NRLLLTG. Protein Sci. *12*, 2588–2596. https://doi.org/10.1110/ps.03269103.
38. Takenaka, I.M., Leung, S.-M., McAndrew, S.J., Brown, J.P., and Hightower, L.E. (1995). Hsc70-binding Peptides Selected from a Phage Display Peptide Library that Resemble Organellar Targeting Sequences (*). J. Biol. Chem. *270*, 19839–19844. https://doi.org/10.1074/jbc.270.34.19839.
39. Fontaine, S.N., Martin, M.D., Akoury, E., Assimon, V.A., Borysov, S., Nordhues, B.A., Sabbagh, J.J., Cockman, M., Gestwicki, J.E., Zweckstetter, M., and Dickey, C.A. (2015). The active Hsc70/tau complex can be exploited to enhance tau turnover without damaging microtubule dynamics. Hum. Mol. Genet. *24*, 3971–3981. https://doi.org/10.1093/hmg/ddv135.
40. Karagoz, G.E., and Rudiger, S.G. (2016). Hsp90 interaction with clients. Trends Biochem. Sci. *40*, 117–125.
41. Morán Luengo, T., Mayer, M.P., and Rüdiger, S.G.D. (2019). The Hsp70–Hsp90 Chaperone Cascade in Protein Folding. Trends Cell Biol. *29*, 164–177. https://doi.org/10.1016/j.tcb.2018.10.004.
42. Mayer, M.P. (2013). Hsp70 chaperone dynamics and molecular mechanism. Trends Biochem. Sci. *38*, 507–514. https://doi.org/10.1016/j.tibs.2013.08.001.
43. Assimon, V.A., Gillies, A.T., Rauch, J.N., and Gestwicki, J.E. (2013). Hsp70 Protein Complexes as Drug Targets. Curr. Pharm. Des. *19*, 404–417.
44. Li, X., Colvin, T., Rauch, J.N., Acosta-Alvear, D., Kampmann, M., Dunyak, B., Hann, B., Aftab, B.T., Murnane, M., Cho, M., et al. (2015). Validation of the Hsp70–Bag3 Protein–Protein Interaction as a Potential Therapeutic Target in Cancer. Mol. Cancer Ther. *14*, 642–648.
45. Rauch, J.N., Zuiderweg, E.R.P., and Gestwicki, J.E. (2016). Non-canonical Interactions between Heat Shock Cognate Protein 70 (Hsc70) and Bcl2-associated Anthanogene (BAG) Co-Chaperones Are Important for Client Release. J. Biol. Chem. *291*, 19848–19857.
46. Mayer, M.P., and Bukau, B. (2005). Hsp70 chaperones: cellular functions and molecular mechanism. Cell. Mol. Life Sci. *62*, 670–684.
47. Zhuravleva, A., Clerico, E.M., and Gierasch, L.M. (2012). An Interdomain Energetic Tug-of-War Creates the Allosterically Active State in Hsp70 Molecular Chaperones. Cell *151*, 1296–1307. https://doi.org/10.1016/j.cell.2012.11.002.
48. Zuiderweg, E.R.P., Hightower, L.E., and Gestwicki, J.E. (2017). The remarkable multivalency of the Hsp70 chaperones. Cell Stress Chaperones *22*, 173–189. https://doi.org/10.1007/s12192-017-0776-y.
49. Taylor, I.R., Assimon, V.A., Kuo, S.Y., Rinaldi, S., Li, X., Young, Z.T., Morra, G., Green, K., Nguyen, D., Shao, H., et al. (2020). Tryptophan scanning mutagenesis as a way to mimic the compound-bound state and probe the selectivity of allosteric inhibitors in cells. Chem. Sci. *11*, 1892–1904. https://doi.org/10.1039/C9SC04284A.
50. Gutierres, M.B.B., Bonorino, C.B.C., and Rigo, M.M. (2020). ChaperISM: improved chaperone binding prediction using position-independent scoring matrices. Bioinformatics *36*, 735–741. https://doi.org/10.1093/bioinformatics/btz670.
51. Chen, X., Hutchinson, R.B., and Cavagnero, S. (2023). Distribution and solvent exposure of Hsp70 chaperone binding sites across the Escherichia coli proteome. Proteins *91*, 665–678. https://doi.org/10.1002/prot.26456.
52. Clerico, E.M., Meng, W., Pozhidaeva, A., Bhasne, K., Petridis, C., and Gierasch, L.M. (2019). Hsp70 molecular chaperones: multifunctional allosteric holding and unfolding machines. Biochem. J. *476*, 1653–1677. https://doi.org/10.1042/BCJ20170380.
53. Liu, Y., Elnatan, D., Sun, M., Myasnikov, A.G., and Agard, D.A. (2020). Cryo-EM reveals the dynamic interplay between mitochondrial Hsp90 and SdhB folding intermediates. Preprint at bioRxiv. https://doi.org/10.1101/2020.10.06.327627.

54. Noddings, C.M., Wang, R.Y.-R., Johnson, J.L., and Agard, D.A. (2022). Structure of Hsp90–p23–GR reveals the Hsp90 client-remodelling mechanism. Nature *601*, 465–469. https://doi.org/10.1038/s41586-021-04236-1.

55. Wang, R.Y.-R., Noddings, C.M., Kirschke, E., Myasnikov, A.G., Johnson, J.L., and Agard, D.A. (2022). Structure of Hsp90–Hsp70–Hop–GR reveals the Hsp90 client-loading mechanism. Nature *601*, 460–464. https://doi.org/10.1038/s41586-021-04252-1.

56. Ferreiro, D.U., Komives, E.A., and Wolynes, P.G. (2018). Frustration, function and folding. Curr. Opin. Struct. Biol. *48*, 68–73. https://doi.org/10.1016/j.sbi.2017.09.006.

57. Vaughan, C.K., Gohlke, U., Sobott, F., Good, V.M., Ali, M.M.U., Prodromou, C., Robinson, C.V., Saibil, H.R., and Pearl, L.H. (2006). Structure of an Hsp90-Cdc37-Cdk4 complex. Mol. Cell *23*, 697–707.

58. Oberoi, J., Guiu, X.A., Outwin, E.A., Schellenberger, P., Roumeliotis, T.I., Choudhary, J.S., and Pearl, L.H. (2022). HSP90-CDC37-PP5 forms a structural platform for kinase dephosphorylation. Nat. Commun. *13*, 7343. https://doi.org/10.1038/s41467-022-35143-2.

59. Keramisanou, D., Vasantha Kumar, M.V., Boose, N., Abzalimov, R.R., and Gelis, I. (2022). Assembly mechanism of early Hsp90-Cdc37-kinase complexes. Sci. Adv. *8*, eabm9294. https://doi.org/10.1126/sciadv.abm9294.

60. Arhar, T., Shkedi, A., Nadel, C.M., and Gestwicki, J.E. (2021). The interactions of molecular chaperones with client proteins: why are they so weak? J. Biol. Chem. *297*, 101282. https://doi.org/10.1016/j.jbc.2021.101282.

61. Wu, K., Stull, F., Lee, C., and Bardwell, J.C.A. (2019). Protein folding while chaperone is bound is dependent on weak interactions. Nat. Commun. *10*, 4833.

62. Lopez, A., Dahiya, V., Delhommel, F., Freiburger, L., Stehle, R., Asami, S., Rutz, D., Blair, L., Buchner, J., and Sattler, M. (2021). Client binding shifts the populations of dynamic Hsp90 conformations through an allosteric network. Sci. Adv. *7*, eabl7295. https://doi.org/10.1126/sciadv.abl7295.

63. Lorenz, O.R., Freiburger, L., Rutz, D.A., Krause, M., Zierer, B.K., Alvira, S., Cuéllar, J., Valpuesta, J.M., Madl, T., Sattler, M., and Buchner, J. (2014). Modulation of the Hsp90 chaperone cycle by a stringent client protein. Mol. Cell *53*, 941–953.

64. Rüdiger, S., Freund, S.M.V., Veprintsev, D.B., and Fersht, A.R. (2002). CRINEPT-TROSY NMR reveals p53 core domain bound in an unfolded form to the chaperone Hsp90. Proc. Natl. Acad. Sci. *99*, 11085–11090. https://doi.org/10.1073/pnas.132393699.

65. Seidler, P.M., Shinsky, S.A., Hong, F., Li, Z., Cosgrove, M.S., and Gewirth, D.T. (2014). Characterization of the Grp94/OS-9 Chaperone–Lectin Complex. J. Mol. Biol. *426*, 3590–3605. https://doi.org/10.1016/j.jmb.2014.08.024.

66. Rüdiger, S., Buchberger, A., and Bukau, B. (1997). Interaction of Hsp70 chaperones with substrates. Nat. Struct. Biol. *4*, 342–349. https://doi.org/10.1038/nsb0597-342.

67. Karagöz, G.E., Duarte, A.M.S., Akoury, E., Ippel, H., Biernat, J., Morán Luengo, T., Radli, M., Didenko, T., Nordhues, B.A., Veprintsev, D.B., et al. (2014). Hsp90-Tau complex reveals molecular basis for specificity in chaperone action. Cell *156*, 963–974. https://doi.org/10.1016/j.cell.2014.01.037.

68. Chiosis, G., Digwal, C.S., Trepel, J.B., and Neckers, L. (2023). Structural and functional complexity of HSP90 in cellular homeostasis and disease. Nat. Rev. Mol. Cell Biol. *24*, 797–815. https://doi.org/10.1038/s41580-023-00640-9.

69. Schindelin, J., Arganda-Carreras, I., Frise, E., Kaying, V., Longair, M., Pietzsch, T., Preibisch, S., Rueden, C., Saafeld, S., Schmid, B., et al. (2012). Fiji: an open-source platform for biological image analysis. Nat. Methods. *9*, 676–682. https://doi.org/10.1038/nmeth.2019.

70. Scarabelli, G., Morra, G., and Colombo, G. (2010). Predicting interaction sited from the energetics of isolated proteins: a new approach to epitope mapping. Biophys. J. *98*, 1966–1975.

71. Morra, G., and Colombo, G. (2008). Relationship between energy distribution and fold stability: Insights from molecular dynamics simulations of native and mutant proteins. Proteins *72*, 660–672.

72. Genoni, A., Morra, G., and Colombo, G. (2012). Identification of Domains in Protein Structures from the Analysis of Intramolecular Interactions. J. Phys. Chem. B *116*, 3331–3343.

73. Morra, G., Genoni, A., and Colombo, G. (2014). Mechanisms of Differential Allosteric Modulation in Homologous Proteins: Insights from the Analysis of Internal Dynamics and Energetics of PDZ Domains. J. Chem. Theory Comput. *10*, 5677–5689.

74. Paladino, A., Morra, G., and Colombo, G. (2015). Structural Stability and Flexibility Direct the Selection of Activating Mutations in Epidermal Growth Factor Receptor Kinase. J. Chem. Inf. Model. *55*, 1377–1387. https://doi.org/10.1021/acs.jcim.5b00270.

75. Peri, C., Morra, G., and Colombo, G. (2016). Surface energetics and protein-protein interactions: analysis and mechanistic implications. Sci. Rep. *6*, 24035. https://doi.org/10.1038/srep24035.

76. Torielli, L., Serapian, S.A., Mussolin, L., Moroni, E., and Colombo, G. (2023). Integrating Protein Interaction Surface Prediction with a Fragment-Based Drug Design: Automatic Design of New Leads with Fragments on Energy Surfaces. J. Chem. Inf. Model. *63*, 343–353. https://doi.org/10.1021/acs.jcim.2c01408.

77. Capelli, R., Matterazzo, E., Amabili, M., Peri, C., Gori, A., Gagni, P., Chiari, M., Lertmemongkolchai, G., Cretich, M., Bolognesi, M., et al. (2017). Designing Probes for Immunodiagnostics: Structural Insights into an Epitope Targeting Burkholderia Infections. ACS Infect. Dis. *3*, 736–743. https://doi.org/10.1021/acsinfecdis.7b00080.

78. Bombaci, M., Fassi, E.M.A., Gobbini, A., Mileto, D., Cassaniti, I., Pesce, E., Casali, E., Mancon, A., Sammartino, J., Ferrari, A., et al. (2024). High-throughput peptide array analysis and computational techniques for serological profiling of flavivirus infections: Implications for diagnostics and vaccine development. J. Med. Virol. *96*, e29923. https://doi.org/10.1002/jmv.29923.

79. Case, D.A., Ben-Shalom, I.Y., Brozell, S.R., Cerutti, D.S., Cheatham, T.E., Cruzeiro, V.W.D., Darden, T.A., Duke, R.E., Ghoreishi, D., Gilson, M.K., et al. (2018). AMBER 2018 (University of California).

80. Jorgensen, W.L., Chandrasekhar, J., Madura, J.D., Impey, R.W., and Klein, M.L. (1983). Comparison of simple potential functions for simulating liquid water. J. Chem. Phys. *79*, 926–935.

81. Miyamoto, S., and Kollman, P.A. (1992). SETTLE: An analytical version of the SHAKE and RATTLE algorithms for rigid water models. J. Comput. Chem. *13*, 952–962.

82. Bussi, G., Donadio, D., and Parrinello, M. (2007). Canonical sampling through velocity rescaling. J. Chem. Phys. *126*, 014101. https://doi.org/10.1063/1.2408420.

83. Berendsen, H.J.C., Postma, J.P.M., van Gunsteren, W.F., Di Nola, A., and Haak, J.R. (1984). Molecular dynamics with coupling to an external bath. J. Chem. Phys. *81*, 3684–3690.

84. Meng, E.C., Goddard, T.D., Pettersen, E.F., Couch, G.S., Pearson, Z.J., Morris, J.H., and Ferrin, T.E. (2023). UCSF ChimeraX: Tools for structure building and analysis. Protein Sci. *32*, e4792. https://doi.org/10.1002/pro.4792.

85. Humphrey, W., Dalke, A., and Schulten, K. (1996). VMD: Visual molecular dynamics. J. Mol. Graph. *14*, 33.

86. D'Annessa, I., Moroni, E., and Colombo, G. (2021). Visualizing the Dynamics of a Protein Folding Machinery: The Mechanism of Asymmetric ATP Processing in Hsp90 and its Implications for Client Remodelling. J. Mol. Biol. *433*, 166728. https://doi.org/10.1016/j.jmb.2020.166728.

87. Rinaldi, S., Colombo, G., and Morra, G. (2024). Exploring Mutation-Driven Changes in the ATP-ADP Conformational Cycle of Human Hsp70 by All-Atom MD Adaptive Sampling. J. Phys. Chem. B *128*, 7770–7780. https://doi.org/10.1021/acs.jpcb.4c03603.

88. Mollapour, M., Tsutsumi, S., Donnelly, A.C., Beebe, K., Tokita, M.J., Lee, M.-J., Lee, S., Morra, G., Bourboulia, D., Scroggins, B.T., et al. (2010). Swe1/Wee1-dependent tyrosine phosphorylation of Hsp90 regulates distinct facets of chaperone function. Mol. Cell *37*, 333–343.

STAR★METHODS

KEY RESOURCES TABLE

REAGENT or RESOURCE	SOURCE	IDENTIFIER
Antibodies		
Rabbit anti-HSP70	StressMarq Biosciences	Cat#SPC-103; RRID:AB_2570584
Rat anti-HSP90	Enzo Life Sciences	Cat# ADI-SPA-835-F, RRID:AB_11181205
Mouse anti-GAPDH (D4C6R)	Cell Signaling Technology	Cat# 97166, RRID:AB_2756824
Rabbit anti-Cdc37	StressMarq Biosciences	Cat# SPC-142; RRID:AB_2570605
Rabbit anti-CDK4	Cell Signaling Technology	Cat# 12790, RRID:AB_2631166
Rabbit anti-cleaved-caspase-3(Asp175)	Cell Signaling Technology	Cat# 9661, RRID:AB_2341188
Rabbit Phospho-Rb (Ser807/811)	Cell Signaling Technology	Cat# 8516, RRID:AB_11178658
Mouse anti-Rb	Cell Signaling Technology	Cat# 9309, RRID:AB_823629
Cleaved PARP	Cell Signaling Technology	Cat# 5625; RRID:AB_10699459
Rabbit anti-Cleaved Caspase-8 (Asp391)	Cell Signaling Technology	Cat# 9496, RRID:AB_561381
Anti-mouse secondary	Cell Signaling Technology	Cat# 7076; RRID:AB_330924
Anti-rabbit secondary	Cell Signaling Technology	Cat# 7074; RRID:AB_2099233
Anti-rat secondary	Cell Signaling Technology	Cat# 7077; RRID:AB_10694715
Chemicals, peptides, and recombinant proteins		
Standard Fmoc-protected amino acids-L	Novabiochem	N/A
Standard Fmoc-protected amino acids-D	Sigma-Aldrich	N/A
Wang Resin	Novabiochem	855121
N,N-dimethylformamide (DMF)	Sigma-Aldrich	227056
acetic anhydride	Sigma-Aldrich	320102
Trifluoroacetic acid (TFA)	Carlo Erba	P0082147
N,N-Diisopropylethylamine (DIPEA)	TCI	D1599
Piperidine	Sigma-Aldrich	104094
Pyridine	Sigma-Aldrich	360570
Ethanedithiol (EDT)	Sigma-Aldrich	02390
Triisopropylsilane (TIS)	Sigma-Aldrich	233781
N-hydroxybenzotriazole (HOBt)	Sigma-Aldrich	157260
N,N′-Diisopropyl-carbodiimide (DIC)	Sigma-Aldrich	D125407
DMAP	TCI	D1450
HATU	TCI	A1797
PyBOP	Fluorochem	009017
Biotin	Novabiochem	851209
5-carboxyfluorescein	Novabiochem	851025
DMSO	Sigma-Aldrich	276855
Hsp90	Prodroumou Lab	N/A
Cdc37	Prodromou Lab	M/A
5-FAM-LVEALY	GenScript	N/A
5-FAM-Ahx-LPISTGGFQMALTPVV	GenScript	N/A
Ac-NRLLLTG	GenScript	N/A
Ac-LPISTGGFQMALTPVV	GenScript	N/A
Hsc70 SBD (395-509)	this paper	N/A
CDK4-1	This paper	N/A
CDK4-2	This paper	N/A
CDK4-4	This paper	N/A

(*Continued on next page*)

Continued

REAGENT or RESOURCE	SOURCE	IDENTIFIER
Biotinylated CDK4-2	This paper	N/A
Biotinylated CDK4-4	This paper	N/A
CDK4-2-FAM	This paper	N/A
CDK4-4-FAM	This paper	N/A
Minimal CDK4-2 peptide	This paper	N/A
Critical commercial assays		
Strept agarose	ThermoFisher Scientific	Cat# 20349
Deposited data		
Docking results data	This paper	https://doi.org/10.5281/zenodo.7912736
Experimental models: cell lines		
HEK293	ATCC	Cat# CRL-1573; RRID:CVCL_0045
HK-2	ATCC	Cat# CRL-2190; RRID:CVCL_0302
786-O	ATCC	Cat# CRL-1932; RRID:CVCL_1051
Software and algorithms		
MAESTRO - GLIDE	Schrodinger Inc	https://www.schrodinger.com
AMBER 18	Amber	https://ambermd.org
Xmgrace	Wis Plasma Lab	https://plasma-gate.weizmann.ac.il/Grace/
INPUT FILES for SIMULATIONS of short peptides	This paper	https://doi.org/10.5281/zenodo.16089270
INPUT FILES for SIMULATIONS of Hsp70-peptide Complex	This paper	https://doi.org/10.5281/zenodo.16089407
Docking Data to Hsp70	This paper	https://doi.org/10.5281/zenodo.16088779
Docking Data to Hsp90	This paper	https://doi.org/10.5281/zenodo.16089216
Code for Analysis of Simulations	This paper	https://github.com/colombolab
MLCE code	This paper	https://github.com/colombolab
GraphPad Prism 10	GraphPad	https://www.graphpad.com/scientific-software/prism/
UCSF ChimeraX 1.8	University of California	https://www.rbvi.ucsf.edu/chimerax/
MAESTRO - GLIDE	Schrodinger Inc	https://www.schrodinger.com
AMBER 18	Amber	https://ambermd.org
Fiji (Image J)	Schindelin et al.[69]	https://imagej.net/software/fiji/
Other		
384-well Low Volume Black Round Bottom	Corning	N/A

EXPERIMENTAL MODEL AND STUDY PARTICIPANT DETAILS

Cell lines

HEK293 derived from human fetal tissue were obtained from the ATCC and were grown in Dulbecco's Modified Eagle Medium (DMEM, Sigma-Aldrich). 786-O, human kidney epithelial clear cell adenocarcinoma derived from a white, 58 year old male were obtained from the ATCC and grown in RPMI-1640 (Sigma-Aldrich). All growth media was supplemented with 10% fetal bovine serum (FBS, Sigma-Aldrich) and were maintained in a CellQ incubator (Panasonic Healthcare) at 37°C in an atmosphere containing 5% CO_2.

METHOD DETAILS

Computational methods

Identification of protein unfolding regions with the MLCE algorithm

MLCE (Matrix of Low Energy Couplings) is a technique based on the analysis of the interaction energies of all the amino acids in a protein.[70–74] In the case of the CDK4 kinase studied here, the representative structure of the most populated conformational cluster obtained from the simulations previously described in Paladino et al.[28] was used for energetic analysis. In particular, MLCE computes the non-bonded part of the potential (van der Waals, electrostatic interactions, solvent effects) via a MM/GBSA calculation, obtaining, for a protein composed by N residues, a $N \times N$ symmetric interaction matrix M_{ij}. This matrix can be expressed in terms of its eigenvalues and eigenvectors as

$$M_{ij} = \sum_{\alpha=1}^{N} \lambda_\alpha v_i^\alpha v_j^\alpha$$

where λ_α is the α-th eigenvalue and v_i^α is the i-th component of the corresponding eigenvector. The eigenvector with the most negative correspondent eigenvalue contains most of the interaction information for the stabilizing interaction of the system. In a complementary way, this provides information on the residues that contribute the least to the stabilization of the fold, and are thus most prone to unfold.

An approximated interaction matrix $\tilde{M}_{ij}$ can thus be reconstructed as

$$\tilde{M}_{ij} = \lambda_1 v_i^1 v_j^1$$

If the structure of the protein is known, one can estimate a contact matrix C_{ij} by assuming two amino acids in contact if the distance between two of their heavy atoms is smaller than a 6.5Å threshold. The Hadamard product of the two matrices gives us the matrix of the local coupling energies

$$MLCE_{ij} = \tilde{M}_{ij} \cdot C_{ij}$$

We select as possible unfolding/interacting zones, the sets of residues that are in contact and that show the weakest couplings to the rest of the protein sequence. This analysis has been validated in several instances against known protein-protein complexes,[21,75] in the design of ligands for Protein-Protein Interactions (PPIs),[76] and in the design of epitope mimics.[29,77,78]

Molecular dynamics simulations of designed peptides mimicking unfolding regions on CDK4

Molecular dynamics were run using: Amber18 pmemd.CUDA, with the ff14SB force field under periodic boundary conditions.[79] Peptides were simulated starting from a fully extended conformation, leaving them free to explore conformational space with the minimal possible bias. Before starting the simulations, preliminary steps were taken: the N-terminus was capped with an acetyl group and the C-terminus was capped with an N-methyl group to neutralize their charge. The simulation box was filled with TIP3P water molecules[80] and rendered electroneutral by the addition of sodium or chlorine counterions (depending on the charge of the single peptide). In order to remove any bad contacts between solute and solvent, every system was minimized with 10,000 steps of steepest descent followed by 10,000 steps of conjugate gradient. Solvent equilibration was performed for 9 picoseconds without the use of the SHAKE algorithm.[81] This process was divided into 3 steps: up to step 3000 the temperature has gradually passed from 25 to 400 K, from step 3000 to 6000 has remained stable at 400 K and from step 6000 to 9000 is was cooled. The systems were then heated from 50 K to 300 K in NVP environment running 1.2 nanoseconds of MD with no restraints for C-, with the SHAKE algorithm. The Langevin barostat was used to maintain the temperature constant, and each simulation is independent, as the velocities and coordinates of each simulation were generated randomly.[82] The last step before the start of dynamics was an equilibration step: using the Langevin thermostat the temperature is kept constant at 300 K, while the pressure is maintained at 1 bar with the Berendsen barostat.[83] Each peptide was solvated in a cubic box and an 11 Å layer of solvent molecules surrounding the peptide was added. In total, 40 independent replicates were run for 600 ns seconds each, yielding a total of 24 μs for each system.

In the case of the Hsp70-peptide complex described in the results section, the same preparation and equilibration protocol was used. In this case, 8 independent replicas, each covering a timespan of 1 microsecond, were run. The resulting trajectories were then combined into a single metatrajectory, which was then analyzed to identify the stable contacts between the peptide and the chaperone SBD.

Visual representation and analysis of the simulations were carried out using ChimeraX,[84] Visual Molecular Dynamics (VMD) software[85] and Maestro (www.schrodinger.com).

MSM

Markov State Models (MSMs) to explore the energetics of **Cdk4-2** and **Cdk4-4** were carried out using the dedicated python package PyEMMA for all steps (up to model validation and analysis).[86] To begin with, the 40 MD production replicates for each variant were combined into full 24 μs meta-trajectories, aligning structures on backbone heavy atoms of residues forming secondary structures, as recognized by PyMOL. Such a long total simulation time was deemed necessary to explore sufficient conformational space.

We ranked eight different featurization by means of the VAMP2 score which measures the kinetic variance contained in the collected features. We consistently founded that C-alpha distances + minimum side chain distance and C-alpha distances + residues-COM distances were performing the best for **Cdk4-2** and **Cdk4-4** respectively. Then, we performed a more detailed VAMP2 score analysis for the chosen input features by varying the dimension parameter for several lag times. The lag time has been chosen based on the best trade-off to simultaneously maximize the VAMP2 score and minimize the number of tICA components to describe the system. We remapped our input features into time-independent components (tICs) using a lag time of 1.4 and 0.2 ns for **Cdk4-2** and **Cdk4-4** respectively. We subsequently ascertained that a k-means clustering run with k = 800 and 600 cluster centers (**Cdk4-2** and **Cdk4-4**, respectively) was sufficient to crisply discretize the coordinate subspace spanned by the tICs into as many conformational "microstates". We finally proceeded to build MSMs on these tIC-clustered trajectories, using a model lag time of 2.8 ns and 4 ns, and considering 3 and 2 kinetically accessible metastable macrostates (**Cdk4-2** and **Cdk4-4**, respectively). Validity of these criteria was confirmed as the deriving models passed the Chapman-Kolmogorov test for markovianity (see Figure S1). Thermodynamic and kinetic data pertaining to the macrostates of both peptides featured in these MSMs were derived, respectively,

through Perron cluster–cluster analysis and calculation of mean first passage times. As a final validation criterion, we noted that MSMs built with the same criteria but starting from different random seeds yielded comparable results.

Molecular docking

The Glide module of the Maestro software suite from Schrödinger was used for this analysis (www.schrodinger.com). Several molecular docking runs were carried out: a preliminary phase in which we performed an extra precision docking (XP) on the four most representative cluster conformations of Hsp90 obtained from the MD simulations of the full length Hsp90/Cdc37/CDK4 complex, previously described in D'Annessa et al.[86] For Hsp70, we used the model described in Rinaldi et al.[87] The four main representative structures of Hsp70 on which docking was run were also selected from this simulation.

For docking designed peptides into both Hsp90 and Hsp70 client binding sites, a receptor grid was built to fit the pocket taken into consideration, and 10,000 poses were calculated for the initial docking phase, of which the best 1,000 poses per peptide were saved for energy minimization. The output in this first phase was of one pose per peptide. From this first study, the best poses were isolated. Only one pose is shown in Figures 2 and 7, but similar patterns were observed in the others.

Experimental details

Cell lines

HEK293 cells were grown in Dulbecco's Modified Eagle Medium (DMEM, Sigma-Aldrich) and 786-O cells were grown in RPMI-1640 (Sigma-Aldrich). All growth media was supplemented with 10% fetal bovine serum (FBS, Sigma-Aldrich) and were maintained in a CellQ incubator (Panasonic Healthcare) at 37°C in an atmosphere containing 5% CO_2. All cells were acquired from (American Type Culture Collection, ATCC).

Protein extraction from mammalian cells

Protein extraction from mammalian cells was carried out using methods previously described.[88] Adherent cells were washed once with ice cold PBS and lysed with 200 μl lysis buffer (20 mM Tris-HCl (pH 7.4), 100 mM NaCl, 1 mM $MgCl_2$, 0.1% NP40, protease inhibitor cocktail (Roche), and PhosSTOP (Roche)). Cells were sonicated for 3 sec prior to being centrifuged at 4°C, 14,000 rpm for 8 mins to pellet cell debris. The supernatant was transferred to a fresh tube and stored at -80°C or used in downstream assays.

Pulldown and western blotting

Protein lysate was quantified using Bradford Assay (Bio-Rad). For Western Blotting, equal amounts of protein were run on SDS-PAGE gel and separated proteins were transferred to nitrocellulose membrane using TransBlot Turbo (Bio-Rad). For pulldown, cell lysate was incubated with indicated amounts of biotinylated-peptide 1 hr at 4°C prior to incubation with streptavidin-agarose beads for 1 hr at 4°C. Proteins bound to beads were washed with lysis buffer 4 times and eluted in 5x Laemmli buffer. Precipitated proteins were separated by SDS-PAGE and transferred to nitrocellulose membranes as above. Co-precipitated proteins and inputs were detected by immunoblotting with antibodies recognizing cleaved-caspase 3, phospho-S807/S811-Rb, Rb, CDK4, GAPDH, Cdc37 (Cell Signalling Technology), Hsp70 (StressMarq Biosciences), and Hsp90 (Enzo Life Sciences). Secondary antibodies raised against mouse, rabbit, and rat were purchased from Cell Signaling Technology.

Mass spectrometry analysis

Biotinylated-peptide pulldown was performed as above. Precipitated proteins were separated by SDS-PAGE and stained using Imperial Protein Stain (Thermo Scientific). Selected visible bands were manually cut into small pieces approximately 1 mm x 1 mm and in-gel digested with chymotrypsin, desalted and subjected to LC-MS/MS. The mass spec data was processed by MaxQuant and proteins were identified by database searching with Uniprot human database. Data are presented in Table S3.

Fluorescence microscopy

Cells were plated in 6-well plates and grown overnight to 50% confluency and then treated either with or without fluorescent peptides 37°C for 4 hr. DMSO was used as a control Live cells visualized and imaged with ZOE Fluorescent Cell Imager (Bio-Rad) using transwell and FITC filters.

^{19}F NMR binding experiments

All the NMR experiments were recorded at 25°C with a Bruker FT NMR AvanceNeo 600-MHz spectrometer equipped with a 5-mm CryoProbe QCI ^{1}H/^{19}F-^{13}C/^{15}N-D-Z quadruple resonance with shielded z-gradient coil, and the automatic sample changer SampleJet™ with temperature control. The solubility, purity and stability of ^{19}F-peptides in buffer solution was checked testing them at different concentrations (10, 50 and 100 μM) by ^{1}H and ^{19}F NMR spectroscopy. The binding was evaluated by ^{19}F T_2 filter NMR experiments testing the ^{19}F-peptide (alone and in mixture at 10 or 20 μM) in the absence and in presence of Hsp90 (4 and 10 μM) and Cdc37 (5 μM) in 50 mM tris pH 7.4, 150 mM NaCl, 2mM DTT, DMSO*d6* tot 1% (5ul tot), 10% D_2O (for the lock signal); the total amount of DMSOd_6 in each sample was 1%. The titration experiments were conducted testing the 3 peptides (**Cdk4-2**, **Cdk4-4** and **Cdk4-2-scr**) at 20 μM in the absence and in presence of increasing concentration of Cdc37 (0.5, 1, 2, 4 μM). For all samples a 1D ^{1}H spectrum with water suppression was obtained using the standard NOESY (nuclear Overhauser effect spectroscopy) preset Bruker pulse sequence, with 64 k data points, a spectral width of 30 ppm, 64 scans, an acquisition time of 1.84 s, a relaxation delay (d1) of 4 s and a mixing time of 100 μs. ^{19}F T_2 filter NMR experiments for the binding to Cdc37 and for the titration assays, were recorded by spin-echo scheme (cpmg) with 128 scans, a d1 of 5 s, proton decoupling during the acquisition period a total τ = 0, 0.20 s. The ^{19}F T_2 filter NMR experiments for the binding to Hsp90, were recorded by spin-echo scheme (cpmg) with 512 scans, a d1 of 5 s, proton decoupling during the acquisition period a total τ = 0, 0.12 s The data were multiplied by an exponential function of 1 Hz prior to Fourier transformation. The reference standard in the ^{19}F spectra was $CFCl_3$.

Hsc70 SBD protein

The Hsc70 SBD construct (residues 395–509) was expressed in *E. coli* BL21(DE3) Rosetta cells from a pMCSG7 vector with N-terminal 6-His tag and TEV protease cleavable linker. Liter cultures of TB were grown at 37°C until the A_{600} reached 0.7. Cultures were then cooled to 20°C, induced with 200 μM isopropyl beta-D-1-thiogalactopyranoside (IPTG), and grown overnight at 20°C. Cell pellets were resuspended in His-binding buffer (50 mM Tris pH 8.0, 10 mM imidazole, 500 mM NaCl) supplemented with cOmplete EDTA-free protease inhibitor cocktail (Sigma-Aldrich). Cells were lysed by sonication and pelleted by centrifugation, and the supernatant was then filtered with a 0.22 μm polyethersulfone (PES) membrane. Filtered supernatant was then applied to a 5-mL Ni-NTA Superflow prepacked column (QIAGEN). The column was washed with His-binding buffer, followed by His-washing buffer (50 mM Tris pH 8.0, 30 mM imidazole, 300 mM NaCl), and protein was then eluted off with His-eluting buffer (50 mM Tris pH 8.0, 300 mM Imidazole, 300 mM NaCl). The protein was then further purified by size exclusion chromatography using an AKTA Pure chromatography instrument (Cytiva) using Superdex 75 column (Cytiva) in HEPES buffer (25 mM HEPES pH 7.5, 5 mM $MgCl_2$, 10 mM KCl).

Fluorescence polarization

All FP experiments were performed in 384-well, black, low-volume, round-bottom plates at a final assay volume of 18 μL (Corning 4511). Initial screens using FAM-LVEALY tracer were performed on a Spectramax M5 plate reader (Molecular Devices) measuring at an excitation wavelength of 485 nm and an emission wavelength of 535 nm, with 100 flashes per read. Follow up screens using FAM-Cdk4-2 tracer were performed on a Synergy H4 plate reader (BioTek) measuring excitation wavelength of 485/20 nm and emission wavelength of 528/20 nm. Polarization values reported as millipolarization units (mP). For direct binding, FAM-LVEALY (10 nM) or FAM-Ahx-LPISTGGFQMALTPVV (1 nM) peptides were incubated with varying concentrations of Hsc70 SBD in assay buffer (25 mM HEPES pH 7.4, 20 mM KCl, 6 mM $MgCl_2$, 0.01% Tween-20). The plate was stored in the dark and incubated at room temperature for at least 30 minutes before reading. For competition experiments with the FAM-LVEALY, a mixture of Hsc70 SBD (1 μM) and tracer (10 nM), was incubated with 2X dilutions of peptide (starting at 100 μM). For the experiments using FAM-Cdk4-2 assays, a mixture of 300 nM Hsc70 SBD and 3 nM tracer was incubated with the same 2X dilutions of 100 μM peptide. Incubations occurred in FP Assay buffer with a final 2% DMSO concentration.

Peptide synthesis: General procedures

Materials

N-α-Fmoc-L-amino acids, ethyl cyanoglyoxylate-2-oxime (Oxyma) and building blocks used during chain assembly were purchased from Iris Biotech GmbH (Marktredwitz, Germany). *N,N′*-dimethylformamide (DMF) and trifluoroacetic acid (TFA) were from Carlo Erba (Rodano, Italy). HMPB resin, N,N′-diisopropylcarbodiimide (DIC), dichloromethane (DCM) and all other organic reagents and solvents, unless stated otherwise, were purchased in high purity from Sigma-Aldrich (Steinheim, Germany). All solvents for solid-phase peptide synthesis (SPPS) were used without further purification. HPLC grade acetonitrile (ACN) and ultrapure 18.2 Ω water (Millipore-MilliQ) were used for the preparation of all buffers for liquid chromatography. The chromatographic columns were from Phenomenex (Torrance CA, USA). HPLC eluent A: 97.5% H_2O, 2.5% ACN, 0.7%TFA; HPLC eluent B: 30% H_2O, 70% ACN, 0.7%TFA.

Resin loading

Resin (0.5 mmol/g loading) was swollen in CH_2Cl_2 for 30 min then washed with DMF (3 × 3 mL). A solution of entering Fmoc-amino acid, DIC and Oxyme (5:5, 5 eq over resin loading) and 5% of DMAP in DMF (3 mL) was added and the resin shaken at rt for 4 h. The resin was washed with DMF (2 × 3 mL) and capping was performed by treatment with acetic anhydride/DIEA in DCM (1 x 30 min). The resin was then washed with DMF (2 × 3 mL), CH_2Cl_2 (2 × 3 mL), and DMF (2 × 3 mL). The resin was subsequently submitted to fully automated iterative peptide assembly (Fmoc-SPPS).

Peptide assembly via iterative fully automated microwave assisted SPPS

Peptides were assembled by stepwise microwave-assisted Fmoc-SPPS on a Biotage ALSTRA Initiator+ peptide synthesizer, operating in a 0.1 mmol scale. Activation of entering Fmoc-protected amino acids (0.3M solution in DMF) was performed using 0.5M Oxyma in DMF/0.5M DIC in DMF (1:1:1 molar ratio), with a 5-equivalent excess over the initial resin loading. Coupling steps were performed for 10 minutes at 60°C. Fmoc-deprotection steps were performed by treatment with a 20% piperidine solution in DMF at room temperature (1 x 10 min). Following each coupling or deprotection step, peptidyl-resin was washed with DMF (4 × 3.5 mL). Upon complete chain assembly, resin was washed with DCM (5 × 3.5 mL) and gently dried under a nitrogen flow.

Cleavage from the resin

Resin-bound peptide was treated with an ice-cold TFA, TIS, water, thioanisole mixture (90:5:2.5:2.5 v/v/v/v, 4mL). After gently shaking the resin for 2 hours at room temperature, the resin was filtered and washed with neat TFA (2 × 4 mL). The combined cleavage solutions were worked-up as indicated below.

Work-up and purification

Cleavage mixture was concentrated under nitrogen stream and then added dropwise to ice-cold diethyl ether (40 mL) to precipitate the crude peptide. The crude peptide was collected by centrifugation and washed with further cold diethyl ether to remove scavengers. Residual diethyl ether was removed by a gentle nitrogen flow and the crude peptide was purified by RP-HPLC and lyophilized.

For additional experiments with Hsp70, Ala scanning experiments, and minimal sequence identification from **Cdk4-2**, peptides were ordered from GenScript (95% purity by high-performance liquid chromatography). Fluorescence polarization tracer peptides were designed with a 5-carboxyfluorescein (5-FAM) moiety linked to the peptide N terminus *via* a six-carbon spacer (aminohexanoic

acid). Unlabeled peptides were N-terminally acetylated to enhance stability and solubility. Unless specified, peptides bore an unmodified free carboxylate at the C terminus. Peptides were diluted in dimethyl sulfoxide (DMSO) to 5 mM stock solutions and stored at −20°C.

QUANTIFICATION AND STATISTICAL ANALYSIS

Presented data are representative of three replicates (n=3), unless otherwise specified. Densitometry was performed using Photoshop v.23.5.1 to quantify Western blot band signal intensity. All statistical analysis were performed using Microsoft Excel. Statistical significance was ascertained between individual samples using a parametric unpaired t-test or Tukey's multiple comparisons test where indicated. Significance is denoted by asterisks in each Fig.: $*p < 0.05$; $**p < 0.01$; $***p < 0.001$; $****p < 0.0001$. Error bars represent the standard deviation for three independent experiments, unless otherwise indicated.

Structure, Volume *33*

Supplemental Information

Design of multi-target peptide modulators for protein chaperone networks

Luca Torielli, Matteo Castelli, Francesca Milani, Jennifer A. Heritz, Sara J. Cayaban, Jason Hernandez, Stefano A. Serapian, Andrea Magni, Elena Frasnetti, Filippo Doria, Valentina Pirota, Laura A. Wengert, Mark R. Woodford, Giulia Lodigiani, Greta Bergamaschi, Marina Veronesi, Tiziano Bandiera, Stefania Girotto, Antonella Paladino, Chrisostomos Prodromou, Sarah J. Backe, Dimitra Bourboulia, Anselmo Canciani, Cristina Arrigoni, Marco Lolicato, Jason E. Gestwicki, Mehdi Mollapour, and Giorgio Colombo

SUPPLEMENTARY MATERIAL

Design of Multi-Target Peptide Modulators for Protein Chaperone Networks

Luca Torielli[1,†], Matteo Castelli[1,†], Francesca Milani[1,†], Jennifer A. Heritz[2,3,4], Sara J. Cayaban[2,3,4], Jason Hernandez[9], Stefano A. Serapian[1], Andrea Magni[1], Elena Frasnetti[1], Filippo Doria[1], Valentina Pirota[1], , Laura A. Wengert[2,3], Mark R. Woodford[2,3,4], Giulia Lodigiani[5], Greta Bergamaschi[5], Marina Veronesi[6], Tiziano Bandiera[7], Stefania Girotto[6], Antonella Paladino[8], Chrisostomos Prodromou,[10] Sarah J. Backe[2,3], Dimitra Bourboulia[2,3,4], Anselmo Canciani,[11] Cristina Arrigoni[11], Marco Lolicato[11], Jason E. Gestwicki[9,*], Mehdi Mollapour[2,3,4,*] and Giorgio Colombo[1,*]

Table of Contents:

Supplementary Figure S1, Related to Figure 2. Validation of Markov State Models and Corresponding Free Energy Surfaces.

Supplementary Figure S2, Related to Figure 2. Bound peptides resemble the conformation of known clients.

Supplementary Figure S3, Related to Figure 3. Identifying CDK4 peptide-binding proteins in cell lysates and replicates of Western blots.

Supplementary Figure S4, Related to Figure 4. NMR-investigation of peptide solubility and stability.

Supplementary Figure S5, Related to Figure 3,4. Verification of Cdk4-2 binding to Hsp90 and Cdc37 by Microscale Thermophoresis (MST).

Supplementary Figure S6 Related to Figure 4. Scrambled Cdk4-2 does not bind to Cdc37, as indicated by NMR.

Table S1: Mass spectrometry results from Cdk4-2 pulldown experiments.

Supplemental Methods: RP-HPLC analysis and purification of synthetic peptides.

Supplemental Methods: Electro-spray ionization mass spectrometry (ESI-MS) to characterize synthetic peptides.

Table S2: List of ^{18}F-labeled peptides.

Table S3: Mass-spec analysis results for synthesized peptides**.**

MSM

To put conformational observations on a more quantitative ground and to elucidate the energetics of the distinctive states, we took advantage of the extensive MD sampling for the Cdk4-2 and Cdk4-4 peptide (24 μs each) to construct Markov state models (MSMs) interconnecting diverse conformational states of Cdk4-2 and Cdk4-4.

Cdk4-2

Starting from the entire 24 μs MD metatrajectory of Cdk4-2, we selected C-alpha distances + minimum side chain distance as input features to build the MSM. The selection of these features was guided by the analysis of VAMP2 score and by the need to balance a detailed representation of conformational transitions with their direct physical interpretability. We identified the components (tICs) that capture the slowest collective motions of the system through time-lagged independent components analysis (tICA, lagtime 1.4 ns). On these tICs, we managed to construct a MSM that recognizes three macrostates (Figure S1; see Methods section). As the lowest energy state (0.40 ± 0.67 G/kBT), the MSM identifies the S3 microstate. There then follows other two macrostates S1 and S2 with energies of 1.39 ± 0.25 and 2.53 ± 0.08 G/kBT respectively. For further reference, the reweighted free energy surface of our MSM, plotted along tICs 1 and 2, is illustrated in Figure S1.

Cdk4-4

Starting from molecular dynamics simulations of Cdk4-4, we analyzed its entire 24 μs metatrajectory using C-alpha distances + residues-COM (center of mass) distances as input features. The selection of these features was guided by the analysis of VAMP2 score (see Methods section) and by the need to balance a detailed representation of conformational transitions with their direct physical interpretability. Through time-lagged (0.2 ns lagtime) independent component analysis (tICA), we identified the components (tICs) that capture the slowest collective motions of the system. These tICs were subsequently employed to construct a Markov state model (MSM), which recognizes two macrostates (Figure S1; see Methods section), with the lowest-energy state (0.05 ± 0.95 G/kBT) corresponding to the S2 microstate. Higher-energy macrostate includes S1 with an energy of 3.10 ± 0.05 G/kBT. To provide further insights, the reweighted free energy surface along tICs 1 and 2 is depicted in Figure S1.

Cdk4-2 MSM

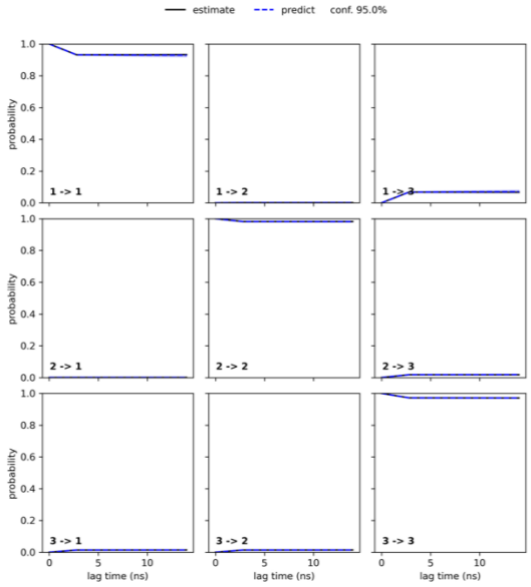

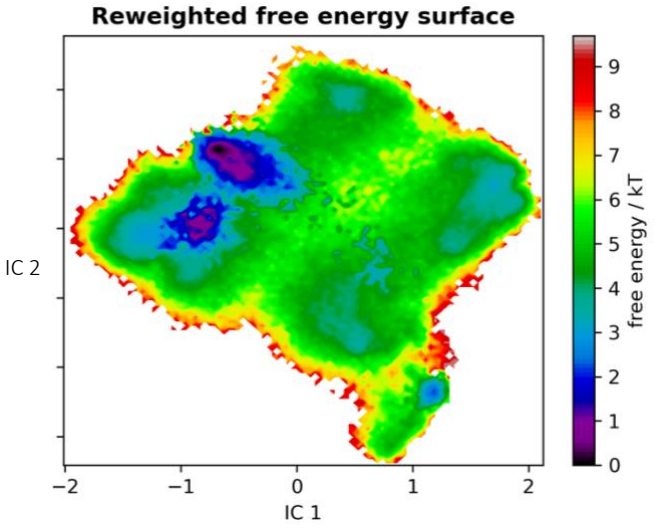

Cdk4-4 MSM

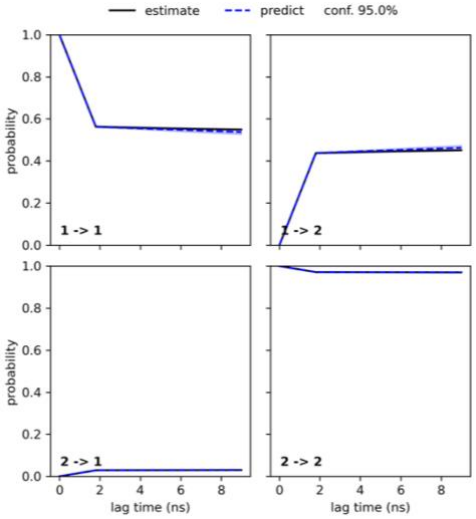

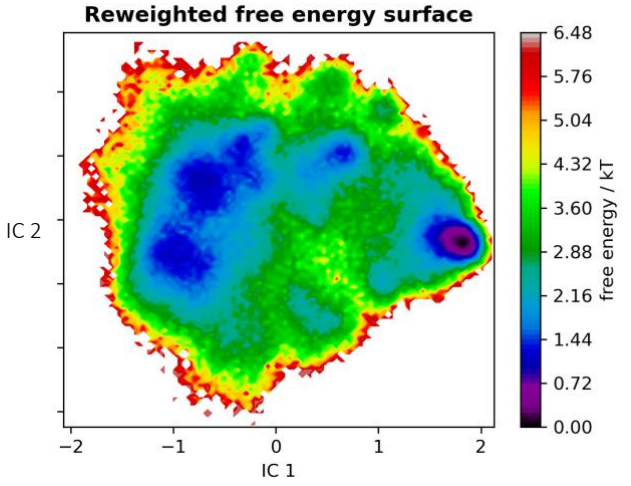

Supplementary Figure S1. Validation of Markov State Models and Corresponding Free Energy Surfaces. Reweighted free energy surfaces and Chapman-Kolmogorov tests for the two peptide MSMs (Cdk4-2 above and Cdk4-4 below). In both cases, the models display consistent Markovian behavior, as indicated by the good agreement between predicted and estimated transition probabilities.

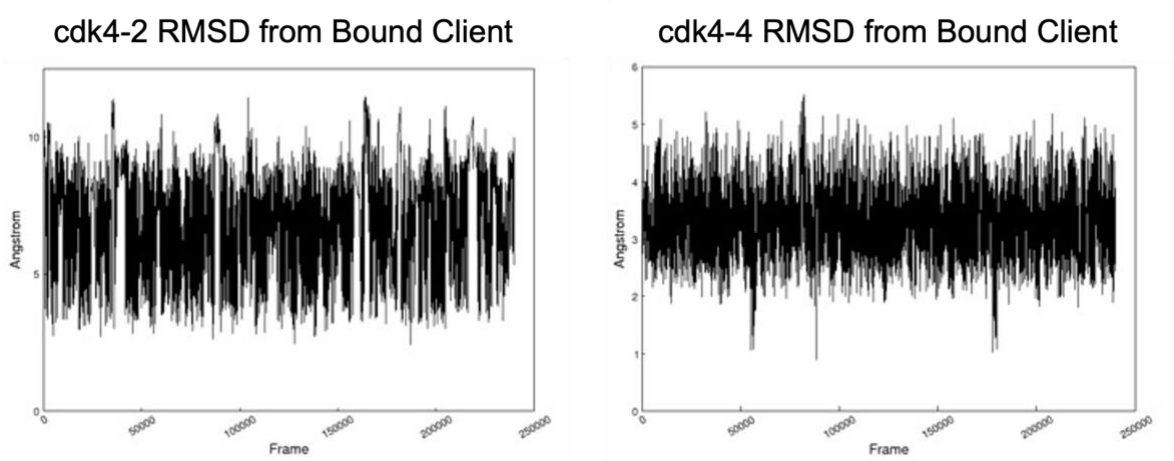

Supplementary Figure S2. Bound peptides resemble the conformation of known clients. Time dependent RMSD of designed peptides from bound client structures along MD simulation trajectories.

A)

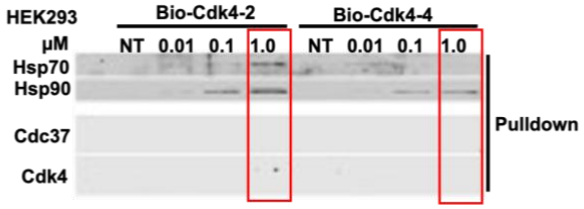

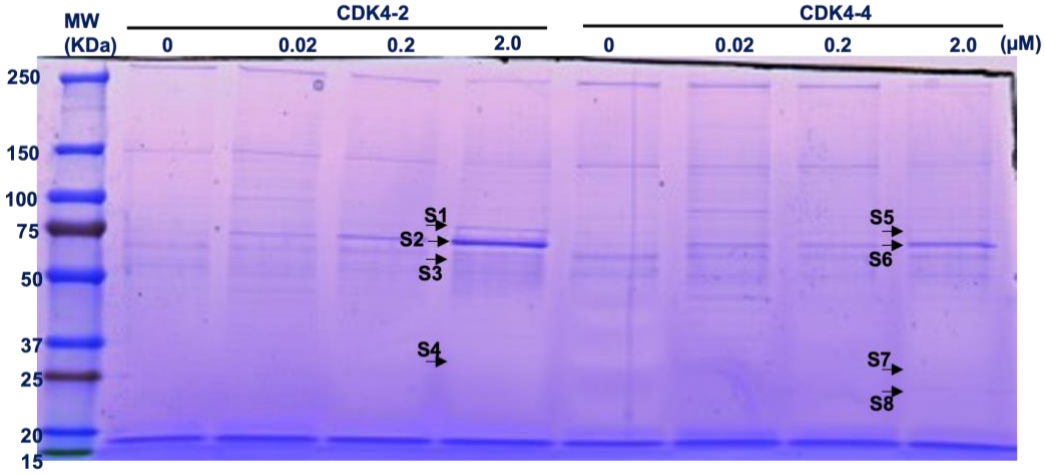

B)

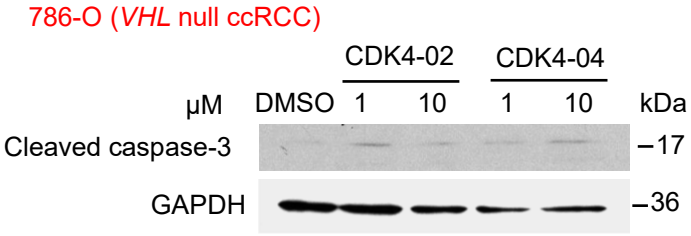

C)

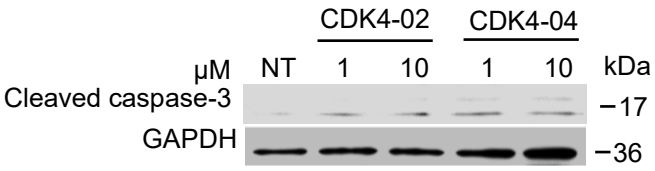

Supplementary Figure S3. Identifying CDK4 peptide-binding proteins in cell lysates.

A) HEK293 cell lysates were incubated with biotinylated **Cck4-2** and **Cdk4-4** peptides for 1 hr prior to incubation with streptavidin-coated agarose beads. Samples were separated by SDS-PAGE and protein was detected by Coomassie staining. The indicated bands were isolated and subject to mass spectrometry.

B) 786-O cells were treated with CDK4-derived peptides for 24 hrs. DMSO was used as control. Induction of apoptosis was evaluated by immunoblotting using cleaved caspase 3 (CCP3) and GAPDH was used as a loading control.

C) HK-2 cells were treated with indicated amount of CDK4 peptides for 24 hrs. DMSO was used as control. Induction of apoptosis was evaluated by immunoblotting using cleaved caspase 3 (CCP3) and GAPDH was used as a loading control.

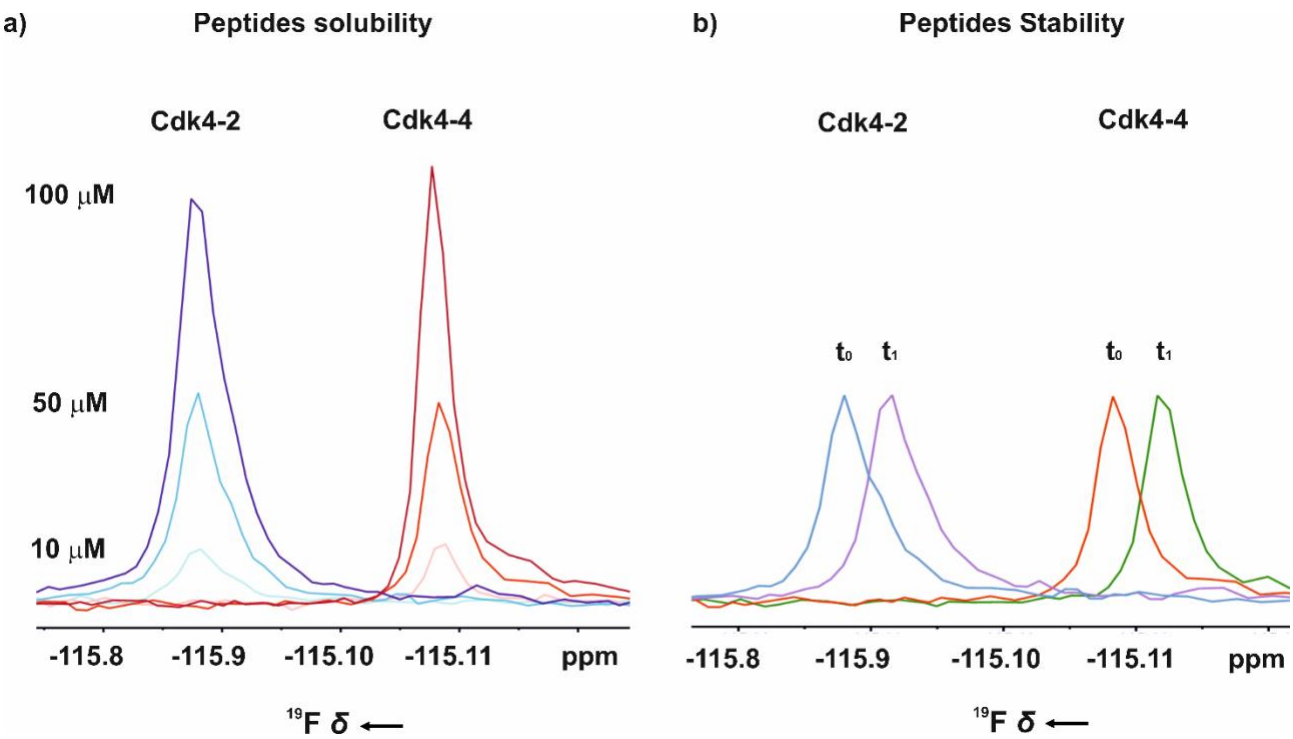

Supplementary Figure S4. NMR-investigation of peptide solubility and stability. a) Superimposition of 1D ^{19}F NMR spectra of **cdk4-2** and CDK4-4 at 10, 50, 100 µM. b) Superimposition of 1D ^{19}F NMR spectra of **cdk4-2** and CDK4-4 at 50 µM recorded just after the samples preparation (t_0) and after 48 hours (t_1).

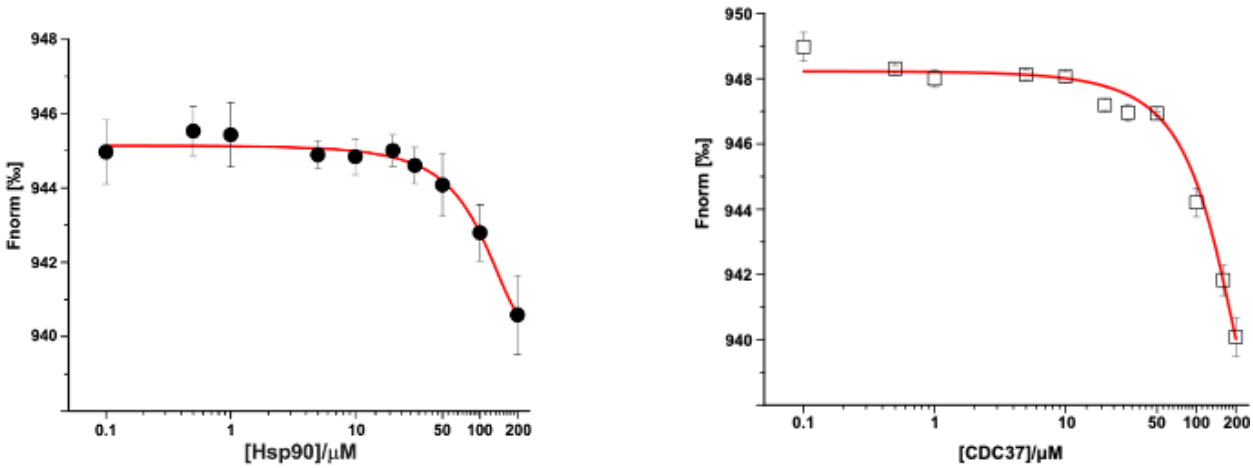

Supplementary Figure S5. . Verification of Cdk4-2 binding to Hsp90 and Cdc37 by Microscale Thermophoresis (MST). Left Panel, filled dots: Analysis of the binding of **Cdk4-2** to purified Hsp90. Average and error bars are calculated from experiments performed in triplicate. **Right Panel, empty squares:** Analysis of the binding of **Cdk4-2** to purified Cdc37. Average and error bars are calculated from experiments performed in triplicate. The error bars are standard deviation of three measurements.

Calculated Kd's **Hsp90**: Kd = 95.4 +/- 20.6; **Cdc37**: Kd = 110.2 +/- 18.1, evaluated with Boltzmann Fit

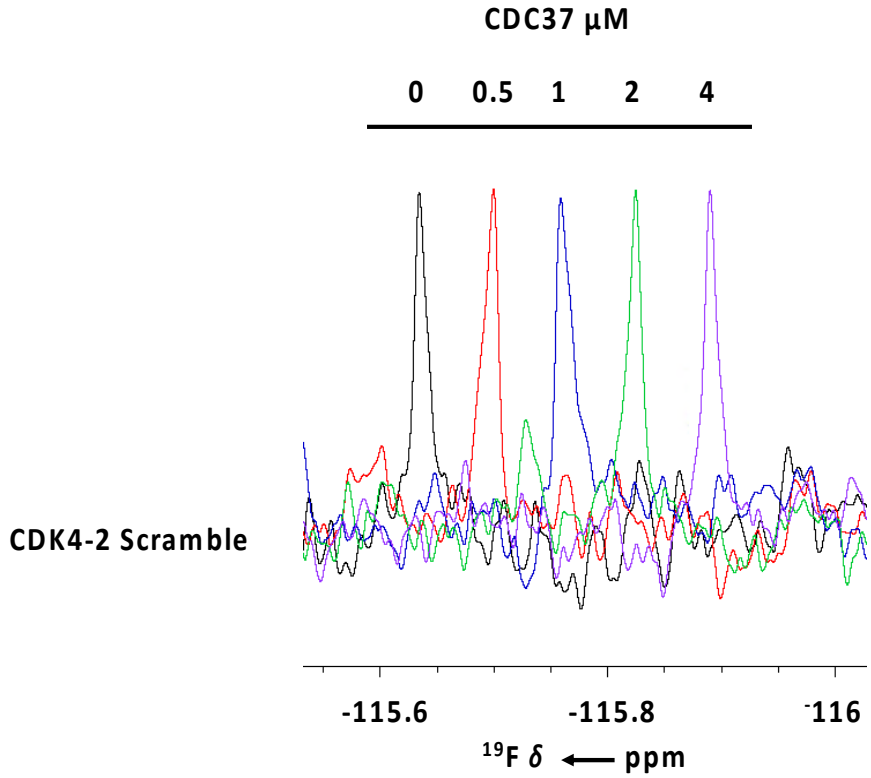

Supplementary Figure S6. Scrambled cdk4-2 does not bind to cdc37, as indicated by NMR. ^{19}F T_2 filter titration experiments of the 20 mM **cdk4-2-scr** peptide in the absence (black) and in presence of increasing concentrations (red, blue and green, violet) of cdc37. The spectra are shifted for a better comparison.

Table S1: Mass spectrometry results from Cdk4-2 pulldown experiments.

Band	Most Abundant Protein	Gene Name
S1	78 kDa glucose-regulated protein	HSPA5
S2	Heat shock 70 kDa protein 1A	HSPA1A
S3	Heat shock 70 kDa protein 1A	HSPA1A
S4	Heat shock 70 kDa protein 1A	HSPA1A
S5	78 kDa glucose-regulated protein	HSPA5
S6	Heat shock 70 kDa protein 1A	HSPA1A
S7	40S ribosomal protein S4	RPS4X
S8	Ig kappa chain V-II region Cum	IGKV A18

PEPTIDE PURIFICATION AND CHARACTERIZATION

RP-HPLC analysis and purification

Analytical RP-HPLC was performed on a Shimadzu Prominence HPLC (Shimadzu) using a Shimadzu Shimpack GWS C18 column (5 micron, 4.6 mm i.d. x 150 mm). Analytes were eluted using a binary gradient of mobile phase A (97.5% H_2O, 2.5% ACN, 0.7%TFA) and mobile phase B (30% H_2O, 70% ACN, 0.7%TFA) using the following chromatographic method: 10% B to 100% B in 14 min; flow rate, 1 ml/min. Preparative RP-HPLC was performed on a Shimadzu HPLC system using a Shimadzu C18 column (10 micron, 21.2 mm i.d. x 250 mm) using the following chromatographic method: 0% B to 100% B in 45 min; flow rate, 14 ml/min. Pure RP-HPLC fractions (>95%) were combined and lyophilized.

Electro-spray ionization mass spectrometry (ESI-MS)

Electro-spray ionization mass spectrometry (ESI-MS) was performed using a Bruker Esquire 3000+ instrument equipped with an electro-spray ionization source and a quadrupole ion trap detector (QITD).

Table S2: List of ^{19}F-labeled peptides.

Code	Sequence
Cdk4_2	LPISTGG**F(F)**QMALTPVV
Cdk4_4	GG**F(F)**QMALTPVV

F(F) = 4-Fluoro-L-phenylalanine

Table S3: Mass-spec analysis results for synthesized peptides.

Code	ESI-MS (m/z) found	ESI-MS (m/z) calculated	Rt
Cdk4_2	1650 (M^+), 825.7 (M^{2+})	1650 (M^+), 825.5 (M^{2+})	11.7 min
Cdk4_4	1138.0 (M^+), 569.8 (M^{2+})	1138.3 (M^+), 569.5 (M^{2+})	11.3 min